that associates with the retinoblastoma protein. J. Biol. Chem. **275:**9797–9804.
27. **Oner, P., S. Bekpinar, F. Cinar, and A. Argun.** 1994. Relationship of some endogenous sex steroid hormones to leukocyte arylsulphatase A activities in pre- and postmenopausal healthy women. Horm. Metab. Res. **26:**301–304.
28. **Oren, M.** 2003. Decision making by p53: life, death and cancer. Cell Death Differ. **10:**431–442.
29. **Paramio, J. M., C. Segrelles, M. L. Casanova, and J. L. Jorcano.** 2000. Opposite functions for E2F1 and E2F4 in human epidermal keratinocyte differentiation. J. Biol. Chem. **275:**41219–41226.
30. **Pelzer, T., M. Schumann, M. Neumann, T. de Jager, M. Stimpel, E. Serfling, and L. Neyses.** 2000. 17β-Estradiol prevents programmed cell death in cardiac myocytes. Biochem. Biophys. Res. Commun. **268:**192–200.
31. **Petrovsky, N., D. Silva, L. Socha, R. Slattery, and B. Charlton.** 2002. The role of Fas ligand in beta cell destruction in autoimmune diabetes of NOD mice. Ann. N. Y. Acad. Sci. **958:**204–208.
32. **Pike, C. J.** 1999. Estrogen modulates neuronal Bcl-xL expression and beta-amyloid-induced apoptosis: relevance to Alzheimer's disease. J. Neurochem. **72:**1552–1563.
33. **Qian, Y. W., and E. Y. Lee.** 1995. Dual retinoblastoma-binding proteins with properties related to a negative regulator of ras in yeast. J. Biol. Chem. **270:**25507–25513.
34. **Qian, Y. W., Y. C. Wang, R. E. Jr. Hollingsworth, D. Jones, N. Ling, and E. Y. Lee.** 1993. A retinoblastoma-binding protein related to a negative regulator of Ras in yeast. Nature **364:**648-652.
35. **Rathmell, J. C., and C. B. Thompson.** 2002. Pathways of apoptosis in lymphocyte development, homeostasis, and disease. Cell **109:**S97–107.
36. **Rogoff, H. A., M. T. Pickering, M. E. Debatis, S. Jones, and T. F. Kowalik.** 2002. E2F1 induces phosphorylation of p53 that is coincident with p53 accumulation and apoptosis. Mol. Cell. Biol. **22:**5308–5318.
37. **Ruuls, S. R., R. M. Hoek, V. N. Ngo, T. McNeil, L. A. Lucian, M. J. Janatpour, H. Korner, H. Scheerens, E. M. Hessel, J. G. Cyster, L. M. McEvoy, and J. D. Sedgwick.** 2001. Membrane-bound TNF supports secondary lymphoid organ structure but is subservient to secreted TNF in driving autoimmune inflammation. Immunity **15:**533–543.
38. **Saegusa, K., N. Ishimaru, K. Yanagi, K. Mishima, R. Arakaki, T. Suda, I. Saito, and Y. Hayashi.** 2002. Prevention and induction of autoimmune exocrinopathy is dependent on pathogenic autoantigen cleavage in murine Sjogen's syndrome. J. Immunol. **169:**1050–1057.
39. **Saito, I., K. Haruta, M. Shimuta, H. Inoue, H. Sakurai, K. Yamada, N. Ishimaru, H. Higashiyama, T. Sumida, H. Ishida, T. Suda, T. Noda, Y. Hayashi, and K. Tsubota.** 1999. Fas ligand-mediated exocrinopathy resembling Sjogren's syndrome in mice transgenic for IL-10. J. Immunol. **162:**2488–2494.
40. **Shirasuna, K., M. Sato, and T. Miyazaki.** 1981. A neoplastic epithelial duct cell line established form an irradiated human salivary gland. Cancer **48:**745–752.
41. **Spyridopoulos, I., A. Sullivan, M. Kearney, J. Isner, and D. Losordo.** 1997. Estrogen-receptor-mediated inhibition of human endothelial cell apoptosis. Estradiol as a survival factor. Circulation **95:**1505–1514.
42. **Stassi, G., and R. De Maria.** 2002. Autoimmune thyroid disease: new models of cell death in autoimmunity. Nat. Rev. Immunol. **2:**195–204.
43. **Szende, B., I. Romics, and L. Vass.** 1993. Apoptosis in prostate cancer after hormonal treatment. Lancet **342:**1422.
44. **Tan, X., and J. Y. J. Wang.** 1998. The caspase-RB connection in cell death. Trends Cell Biol. **8:**116–120.
45. **Vanags, D. M., M. I. Porn-Ares, S. Coppola, D. H. Burgess, and S. Orrenius.** 1996. Protease involvement in fodrin cleavage and phosphatidylserine exposure in apoptosis. J. Biol. Chem. **271:**31075–31085.
46. **Vaute, O., E. Nicolas, L. Vandel, and D. Trouche.** 2002. Functional and physical interaction between the histone methyl transferase Suv39H1 and histone deacetylases. Nucleic Acids Res. **30:**475–481.
47. **Vousden, K. H.** 2000. p53: death star. Cell **103:**691–694.
48. **Wang, K. K., R. Posmantur, R. Nath, K. McGinnis, M. Whitton, R. V. Talanian, S. B. Glantz, and J. S. Morrow.** 1998. Simultaneous degradation of αII- and βII-spectrin by caspase 3 (CPP32) in apoptotic cells. J. Biol. Chem. **273:**22490–22497.
49. **Wang, R. H., C. W. Liu, V. L. Avramis, and N. Berndt.** 2001. Protein phosphatase 1α-mediated stimulation of apoptosis is associated with dephosphorylation of the retinoblastoma protein. Oncogene **20:**6111–6122.
50. **Whitacre, C. C.** 2001. Sex differences in autoimmune disease. Nat. Immunol. **2:**777–780.
51. **Whitacre, C. C., S. C. Reingold, and P. A. O'Looney.** 1999. A gender gap in autoimmunity. Science **283:**1277–1278.
52. **Yu, J. Y., S. L. DeRuiter, and D. L. Turner.** 2002. RNA interference by expression of short-interfering RNAs and hairpin RNAs in mammalian cells. Proc. Natl. Acad. Sci. USA **99:**6047–6052.
53. **Zhang, Q., N. Vo, and R. H. Goodman.** 2000. Histone binding protein RbAp48 interacts with a complex of CREB binding protein and phosphorylated CREB. Mol. Cell. Biol. **20:**4970–4978.
54. **Zhang, Y., B. O'Brien, J. Trudeau, R. Tan, P. Santamaria, and J. P. Dutz.** 2002. In situ β cell death promotes priming of diabetogenic CD8 T lymphocytes. J. Immunol. **168:**1466–1472.

Immunity 24, 165–177, February 2006 ©2006 Elsevier Inc. DOI 10.1016/j.immuni.2005.12.011

CCR7-Dependent Cortex-to-Medulla Migration of Positively Selected Thymocytes Is Essential for Establishing Central Tolerance

Hirotsugu Kurobe,[1,2] Cunlan Liu,[1] Tomoo Ueno,[1,5] Fumi Saito,[1] Izumi Ohigashi,[1] Natalie Seach,[5] Rieko Arakaki,[3] Yoshio Hayashi,[3] Tetsuya Kitagawa,[2] Martin Lipp,[4] Richard L. Boyd,[5] and Yousuke Takahama[1,*]

[1] Division of Experimental Immunology
Institute for Genome Research
University of Tokushima
Tokushima 770-8503
Japan

[2] Department of Cardiovascular Surgery

[3] Department of Oral Molecular Pathology
Institute of Health Biosciences
University of Tokushima
Tokushima 770-8503
Japan

[4] Department of Molecular Tumorgenetics and Immunogenetics
Max-Delbrück Center for Molecular Medicine
Berlin 13125
Germany

[5] Monash Immunology and Stem Cell Laboratories
Monash University
Clayton 3800
Victoria
Australia

Summary

Immature CD4$^+$CD8$^+$ thymocytes, which are generated in the thymic cortex, are induced upon positive selection to differentiate into mature T lymphocytes and relocate to the thymic medulla. It was recently shown that a chemokine signal via CCR7 is essential for the cortex-to-medulla migration of positively selected thymocytes in the thymus. However, the role of the cortex-to-medulla migration in T cell development and selection has remained unclear. The present study shows that the developmental kinetics and the thymic export of mature thymocytes were undisturbed in adult mice lacking CCR7 or its ligands (CCR7L). The inhibition of sphingosine-1-phosphate-mediated lymphocyte egress from the thymus led to the accumulation of mature thymocytes in the cortex of CCR7- or CCR7L-deficient mice, unlike the accumulation in the medulla of normal mice, thereby suggesting that mature thymocytes may be exported directly from the cortex in the absence of CCR7 signals. However, the thymocytes that were generated in the absence of CCR7 or CCR7L were potent in causing autoimmune dacryoadenitis and sialadenitis in mice and were thus incapable of establishing central tolerance to organ-specific antigens. These results indicate that CCR7-mediated cortex-to-medulla migration of thymocytes is essential for establishing central tolerance rather than for supporting the maturation or export of thymocytes.

*Correspondence: takahama@genome.tokushima-u.ac.jp

Introduction

The thymus is an organ that supports the differentiation and selection of T lymphocytes (Miller, 1961; Ritter and Boyd, 1993; Anderson and Jenkinson, 2001). Lymphoid progenitor cells enter the thymus via the surrounding mesenchymal layer before vascularization during fetal development (Bleul and Boehm, 2000) and via blood vessels that are enriched at the cortico-medulla junction in adulthood (Lind et al., 2001). Several chemokines have been suggested to play a crucial role in the positioning of T precursor cells to the subcapsular zone of the outer cortex of the thymus (Plotkin et al., 2003; Misslitz et al., 2004; Benz et al., 2004; Gray et al., 2005; Liu et al., 2005), where immature CD4$^+$CD8$^+$ double-positive (DP) thymocytes are newly generated (Ritter and Boyd, 1993; Takahama et al., 1994). The DP thymocytes crawl through the cortical environment, seeking to encounter the self-MHC-peptide complex expressed by various stromal cells in the cortex, including the cortical thymic epithelial cells (cTEC) (Bousso et al., 2002). Upon TCR engagement by the MHC-peptide ligands, the DP thymocytes stop crawling and initiate the signaling processes for positive and negative selection, which result in further differentiation into CD4$^+$CD8$^-$/CD4$^-$CD8$^+$ single-positive (SP) thymocytes and apoptotic deletion, respectively (Bousso et al., 2002; Palmer, 2003). Concurrently to the differentiation into SP thymocytes, positively selected thymocytes are relocated to the medulla (Ritter and Boyd, 1993; van Ewijk et al., 1994; Witt et al., 2005). The newly generated SP thymocytes are semimature, being functionally incompetent and susceptible to various apoptotic signals including dexamethasone, and undergo further maturation to become mature SP thymocytes that are functional, dexamethasone-resistant, and CD62L^{high}CD69^{low} (Reichert et al., 1986a; Ramsdell et al., 1991; Kishimoto and Sprent, 1997; Gabor et al., 1997; Sheard et al., 2004). The mature SP thymocytes are exported from the thymus via chemotaxis toward sphingosine-1-phosphate (S1P) in the circulation and are systemically distributed as functional yet naive T lymphocytes (Matloubian et al., 2004; Allende et al., 2004). The maturation of SP thymocytes is thought to occur within the medulla (Egerton et al., 1990; Scollay and Godfrey, 1995), and the export to the circulation is thought to occur through the perivascular space in the medulla (Ushiki, 1986; Kato, 1997).

In the thymic medulla, medullary thymic epithelial cells (mTEC) specifically express the nuclear protein AIRE, which is essential for the promiscuous expression of organ-specific self-antigens by mTEC (Zuklys et al., 2000; Gotter and Kyewski, 2004). AIRE deficiency results in autoimmune-polyendocrinopathy-candidiasis ectodermal dystrophy (APECED) in human (Nagamine et al., 1997; Aaltonen et al., 1997) and mouse (Anderson et al., 2002; Liston et al., 2003; Kuroda et al., 2005). Thus, AIRE expressed by mTEC is essential for establishing the central tolerance of T lymphocytes to organ-specific antigens. The molecular mechanisms involved in the differentiation of thymic epithelial progenitor cells into

AIRE-expressing mTEC have remained vague (Blackburn et al., 2002; Farr et al., 2002), although recent analyses have shown that similar to the organogenesis of lymph nodes and Peyer's patches, the NFκB-mediated signals via LTβR, TRAF6, NIK, and relB are critical for the development of the thymic medulla that regulates central tolerance (Burkly et al., 1995; Boehm et al., 2003; Kajiura et al., 2004; Akiyama et al., 2005). It has also been suggested that the thymic medulla contributes to central tolerance by dendritic cells (DCs), which are of hematopoietic origin and are predominantly localized within the thymic medulla (Flotte et al., 1983; Fairchild and Austyn, 1990). The average lifespan of the newly generated SP thymocytes in the thymus is 12 days (Egerton et al., 1990; Scollay and Godfrey, 1995). During this period, the thymic medulla is thought to provide an environment in which the SP thymocytes are induced to mature and are tuned to acquire central tolerance. However, whether the medulla migration of positively selected thymocytes is essential for the maturation of SP thymocytes, for the acquisition of central tolerance, or for the export from the thymus is unclear.

Previous studies with the chemotaxis assay and mRNA measurement showed that CCR7 expression by developing thymocytes is associated with the phenotypic stage of cortex-to-medulla migration, during the development of immature DP thymocytes to mature SP thymocytes (Kim et al., 1998; Campbell et al., 1999). We have recently shown that CCR7 ligands (CCR7L species CCL19 and CCL21) in the thymus are predominantly produced by mTEC and are localized in the medulla, whereas TCR engagement of immature cortical DP thymocytes elevates the cell surface expression of CCR7 (Ueno et al., 2002, 2004). In mice deficient in CCR7 or CCR7L, the mature SP thymocytes are arrested in the cortex and do not accumulate in the medulla (Ueno et al., 2004). These results indicate that the CCR7 signals are essential for the migration of positively selected thymocytes from the cortex to the medulla. By using mice that are deficient in CCR7 or CCR7L, the present study addresses whether T cells may be exported from the thymic cortex without accumulation in the medulla and whether central tolerance to organ-specific self-antigens may be affected by the absence of medulla migration. We show that the pharmacological inhibition of S1P-mediated thymocyte egress in CCR7- or CCR7L-deficient mice results in the accumulation of mature thymocytes in the cortex, suggesting that mature thymocytes may be exported via the S1P-dependent mechanism from the cortex in the absence of CCR7 signals. We also show that in the absence of CCR7-dependent medulla migration, mature thymocytes are incapable of acquiring tolerance to lacrimal and salivary glands and are potent in inducing autoimmune exocrinopathy similar to Sjögren's syndrome.

Results

S1P Blockade Induces Accumulation of Mature Thymocytes in the Thymic Cortex of CCR7- or CCR7L-Deficient Mice

We have previously shown that mice deficient in CCR7 or CCR7L were defective in the cortex-to-medulla migration of thymocytes and that SP thymocytes generated in CCR7L-deficient (*plt/plt*, P/P) or CCR7-deficient (7/7) mice were barely accumulated in the thymic medulla (Ueno et al., 2004). SP thymocytes in these mutant mice appeared normal in terms of frequency and underwent maturation, including TCR responsiveness and formation of surface phenotypes such as CD62L and CD69 (Ueno et al., 2004). In vivo 5-bromo-2-deoxyuridine (BrdU) labeling showed that SP thymocytes and DP thymocytes in these mutant mice were normally generated according to the developmental kinetics (Figure 1A). In addition, intrathymic FITC administration showed that SP thymocytes in CCR7L- or CCR7-deficient mice were normally exported from the adult thymus to the circulation (Ueno et al., 2004). These results indicate that in CCR7L- or CCR7-deficient adult mice, SP thymocytes show normal maturation without medulla accumulation and normal export from the thymus.

The above results suggested the possibility that the mature SP thymocytes generated in CCR7- or CCR7L-deficient mice might be exported from the cortex without migrating into the medulla. In order to examine this possibility, the mice were administered FTY720, an immunosuppressive compound that is phosphorylated in vivo by sphingosine kinases and acts as an S1P mimetic to sequester T lymphocytes in the thymus and lymph nodes (Chiba et al., 1998; Brinkmann et al., 2002). It was previously shown that S1P1, one of the S1P receptors, is expressed by mature SP thymocytes and that S1P1 is required for the egress of T lymphocytes from the thymus and lymph nodes (Matloubian et al., 2004; Allende et al., 2004). Among the thymocyte subpopulations, S1P1 mRNA was highly expressed in SP thymocytes rather than DP or double-negative (DN) thymocytes (Matloubian et al., 2004; Allende et al., 2004; also shown in Figure 1B). Within the SP thymocytes, the S1P1 expression was predominantly detected in the $CD62L^{high}CD69^{low}$ mature subpopulation rather than the $CD62L^{low}CD69^{high}$ semimature subpopulation (Matloubian et al., 2004; also shown in Figure 1B). Similar to S1P1 expression, CCR7 expression was much higher in SP thymocytes than in DP or DN thymocytes (Kwan and Killeen, 2004; Misslitz et al., 2004; also shown in Figure 1B). Unlike S1P1 expression, however, CCR7 expression was detected in $CD62L^{low}CD69^{high}$ semimature thymocytes as well as in $CD62L^{high}CD69^{low}$ mature thymocytes (Figure 1B). The CCR7 mRNA expression levels measured by quantitative RT-PCR analysis agreed with the CCR7 surface expression levels measured by flow cytometry analysis with CCL19-Ig fusion protein (Figures 1C and 1D). $CCR7^{high}TCR\beta^{high}$ thymocytes contained both the $CD62L^{low}CD69^{high}$ semimature compartment and the $CD62L^{high}CD69^{low}$ mature compartment, whereas $CCR7^{negative/low}TCR\beta^{high}$ thymocytes predominantly contained the $CD62L^{low}CD69^{high}$ semimature compartment (Figure 1C). CCR7 expression was higher in $CD62L^{high}CD69^{low}$ mature thymocytes than in $CD62L^{low}CD69^{high}$ semimature thymocytes (Figure 1D). These results indicate that CCR7 expression is detected in both $CD62L^{low}CD69^{high}$ semimature and $CD62L^{high}CD69^{low}$ mature thymocytes, whereas S1P1 expression is detected predominantly in the $CD62L^{high}CD69^{low}$ mature subpopulation,

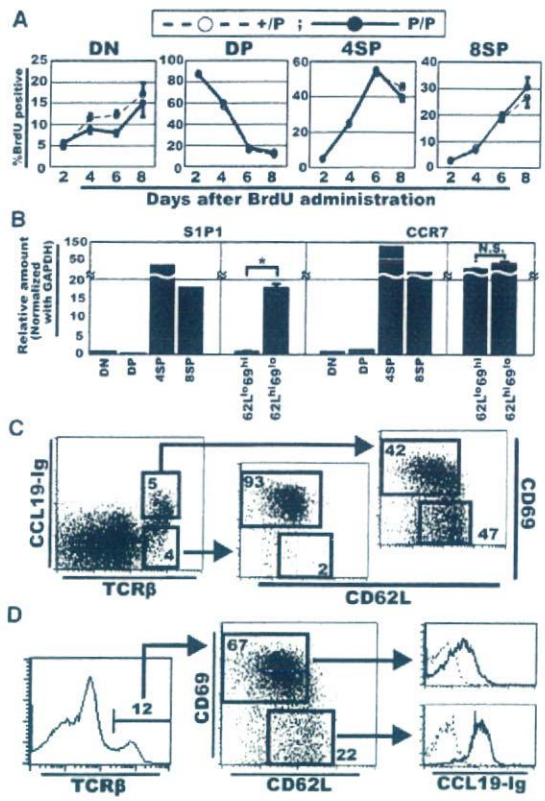

Figure 1. Expression and Function of CCR7 in Thymocyte Subpopulations

(A) Kinetics of mature thymocytes in mice deficient in CCR7L (*plt/plt*, P/P) and their heterozygous control mice (+/P). Thymocytes from BrdU-treated adult mice were stained for CD4, CD8, and BrdU. Plots show means and standard deviations (symbols and bars, respectively; the number of mice used for individual plots ranged from five to seven) of the frequency of BrdU-positive cells within the indicated CD4/CD8 populations of thymocytes on the indicated day of analysis. All the data sets between +/P and P/P groups were not significantly different at all the indicated days of analysis in all of the indicated thymocyte subpopulations (including the data on DN thymocytes) by the Student's t test.

(B) Adult thymocytes from B6 mice were two-color stained for CD4 and CD8 and sorted for DN, DP, CD4SP, and CD8SP populations. Adult B6 thymocytes were also three-color stained for TCRβ, CD62L, and CD69 and were sorted for $TCR\beta^{high}CD62L^{low}CD69^{high}$ semimature and $TCR\beta^{high}CD62L^{high}CD69^{low}$ mature subpopulations. Purity was >97% for CD4/CD8 two-color-sorted fractions and >87% for TCRβ/CD62L/CD69 three-color-sorted fractions. Relative mRNA levels (means and standard errors; n = 3) obtained by quantitative RT-PCR for S1P1 and CCR7, which were normalized to GAPDH mRNA levels, are shown. Asterisk indicates $p < 0.05$ by the Student's t test. N.S., not significant.

(C and D) Adult B6 thymocytes were examined for CCR7 surface expression by using CCL19-Ig, which specifically detects CCR7 on the cell surface. Cells were also stained with PE-labeled anti-TCRβ antibody, FITC-labeled anti-CD62L antibody, and PE-Cy5-labeled anti-CD69 antibody. Where indicated, data were gated for $TCR\beta^{high}CCR7^{high}$ and $TCR\beta^{high}CCR7^{negative/low}$ cells (C) and $TCR\beta^{high}CD62L^{low}CD69^{high}$ and $TCR\beta^{high}CD62L^{high}CD69^{low}$ cells (D). Numbers indicate frequencies of cells within the indicated boxes. Dotted lines indicate control staining profiles without CCL19-Ig. Shown are representative results of four independent measurements.

suggesting that the CCR7-mediated medulla migration and the S1P1-mediated thymocyte egress are differently and sequentially regulated during SP thymocyte maturation.

Importantly, FTY720 treatment induced the accumulation of SP thymocytes in CCR7- or CCR7L-deficient mice as well as in normal mice (Figures 2A and 2B). Among the SP thymocytes, the accumulation was specifically induced in the $CD62L^{high}CD69^{low}$ mature population, in either the CD4SP or the CD8SP compartment (Figures 2A and 2C). Thus, the FTY720-mediated S1P blockade of thymocyte egress to the circulation results in the accumulation of $CD62L^{high}$ mature SP thymocytes even in CCR7- or CCR7L-deficient mice, in which most SP thymocytes are arrested in the cortex and are defective in migrating into the medulla.

It was therefore interesting to identify the location in the thymus where mature thymocytes were accumulating upon FTY720 treatment in CCR7- or CCR7L-deficient mice, as the location for this accumulation would correspond to the microenvironment where S1P would otherwise act to attract mature thymocytes into the circulation. To this end, thymus sections from FTY720-treated mice were stained with mature-thymocyte-specific anti-CD62L antibody and either mTEC-specific ER-TR5 or cTEC-specific ER-TR4 monoclonal antibodies (Figure 3). In agreement with the increase in the $CD62L^{high}$ SP thymocyte population as determined by flow cytometry analysis (Figure 2C), the FTY720 treatment markedly increased the $CD62L^{high}$ thymocyte population in normal mice as well as in CCR7- or CCR7L-deficient mice (Figure 3A). In a parallel analysis of the sections, the increased $CD62L^{high}$ cells were indeed shown to belong to CD4 or CD8 single-positive thymocytes in normal and mutant mice (data not shown), indicating that the $CD62L^{high}$ thymocytes increased in Figure 3A represented mature SP thymocytes. Most remarkably, the FTY720-mediated accumulation of $CD62L^{high}$ mature thymocytes was predominantly detected in the cortex and not the medulla of CCR7- or CCR7L-deficient mice, whereas the $CD62L^{high}$ mature thymocytes were accumulated predominantly in the medulla of control mice (Figure 3A). In the cortex of FTY720-mediated CCR7- or CCR7L-deficient mice and in the medulla of FTY720-mediated control mice, the analysis at higher magnification detected areas where $CD62L^{high}$ thymocytes accumulated around $CD31^+$ endothelial vessels (Figure 3B). In some of those areas, $CD62L^{high}$ thymocytes were found even within the perivascular space surrounded by $CD31^+$ endothelial and $ER\text{-}TR7^+$ mesenchymal cells (Figure 3C). In contrast, no or very few $CD62L^{high}$ thymocytes were found in the medulla of FTY720-treated CCR7- or CCR7L-deficient mice and in the cortex of FTY720-treated control mice (Figures 3A, 3B, and 3C). These results indicate that upon FTY720 treatment, the mature SP thymocytes in CCR7- or CCR7L-deficient mice are accumulated in the cortex rather than the medulla of the thymus and are found even in the cortical perivascular space, suggesting the possibility that mature thymocytes generated in CCR7- or CCR7L-deficient mice may be exported from the cortex through the cortical perivascular space in a S1P-dependent manner.

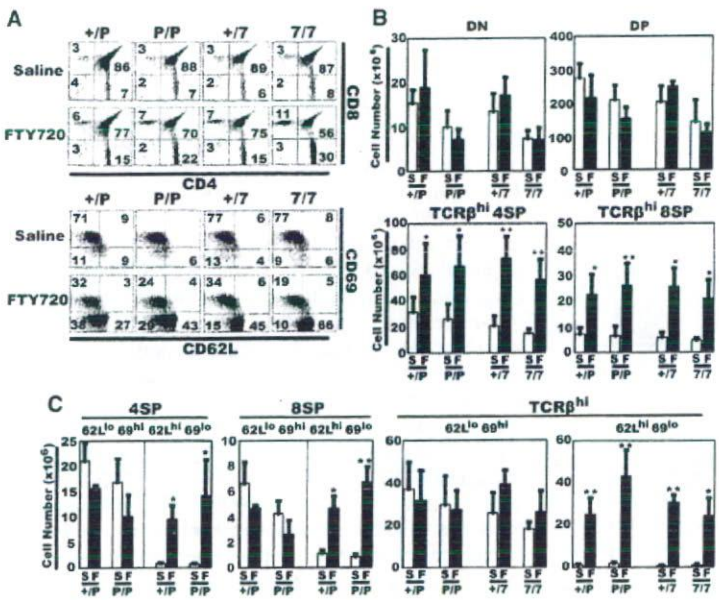

Figure 2. Accumulation of Mature Thymocytes by FTY720-Mediated S1P Blockade

Flow cytometry analysis of thymocytes from CCR7L-deficient mice (*plt/plt*, P/P), CCR7-deficient mice (7/7), and their heterozygous control mice (+/P and +/7), which were treated with either saline (S) or FTY720 (F). The profiles of CD62L and CD69 in (A) were gated for $TCR\beta^{high}$ cells. Numbers in (A) indicate frequencies of cells within the quadrants.

(B and C) Means and standard errors (the numbers of mice analyzed ranged from four to 11 in [B] and three to six in [C]) of the absolute numbers of indicated thymocyte subpopulations are shown. Asterisk indicates $p < 0.05$ and double asterisk indicates $p < 0.005$ by the Student's t test.

Intrathymic Localization of AIRE$^+$ Epithelial Cells and Dendritic Cells in CCR7- or CCR7L-Deficient Mice

We then addressed whether thymic function in inducing central tolerance is affected in CCR7- or CCR7L-deficient mice. It was previously reported that the thymic medulla contributes to establishing central tolerance by AIRE-expressing mTEC (Zuklys et al., 2000; Anderson et al., 2002; Liston et al., 2003; Kuroda et al., 2005) and medulla-localized DCs (Fairchild and Austyn, 1990; Moore et al., 1994). We thus examined whether AIRE$^+$ mTEC and CD11c$^+$ DCs were indeed localized within the medulla in CCR7- or CCR7L-deficient mice. Figure 4 shows that AIRE$^+$ cells in the thymus were predominantly confined in the medullary region in CCR7- or CCR7L-deficient mice as well as in normal mice (Figures 4A and 4B). The analysis at high magnification showed that in the thymus of CCR7- or CCR7L-deficient mice as well as in normal mice, AIRE expression was found in the nuclei, as previously reported (Bjorses et al., 1999; Rinderle et al., 1999), and in a fraction of keratin$^+$MTS-10$^+$ mTEC (Figure 4C). It was also shown that in CCR7- or CCR7L-deficient mice, as in normal mice, CD11c$^+$ DCs were predominantly localized in the medulla, although some CD11c$^+$ DCs were sparsely found in the cortex even in normal mice (Figures 4D and 4E). These results indicate that similar to that of normal mice, AIRE in the thymus of CCR7- or CCR7L-deficient mice are predominantly expressed in the medulla by a fraction of mTEC. The results also show that DCs in the thymus are enriched in the medulla in CCR7- or CCR7L-deficient mice, indicating that CCR7 signals are not required for the accumulation of DCs in the thymic medulla. The results suggest that developing thymocytes in CCR7- or CCR7L-deficient mice, which are not accumulated in the medulla, may fail to directly interact with AIRE$^+$ mTEC.

Thymocytes Generated in CCR7L-Deficient Mice Are Potent in Inducing Autoimmune Exocrinopathy

The above results raised the possibility that the establishment of thymic-medulla-dependent central tolerance to organ-specific antigens might be affected in CCR7- or CCR7L-deficient mice. We thus examined various organs of these mutant mice for lesions that might be associated with defective self-tolerance. As shown in Figure 5, we found that the lacrimal glands, the parotid glands, and the submandibular glands exhibited periductal lymphocyte infiltration in CCR7- or CCR7L-deficient mice (Figures 5A, 5B, and 5C). Lymphocyte infiltration in the lacrimal glands was accompanied by severe tissue damage, including the destruction of acinar cells (Figures 5A and 5D and Figure 6A). In mice up to 25 weeks old, the tissue damage was largely specific for these exocrine glands, as no apparent lesions were detected in other organs, including the trachea, thyroid, liver, spleen, kidney, intestine, adrenal gland, and ovary (data not shown). The lesions in these exocrine glands were detected in all the tested mutant mice ($n = 14$ for *plt/plt* mice; $n = 5$ for CCR7-deficient mice), even as early as 5 weeks old (Figure 5D), and were found similarly in CCR7L-deficient mice of BALB/c background as well as C57BL/6 background (Figures 5A, 5B, and 5C). The infiltrated lymphocytes were mostly CD4$^+$ T cells and B cells, and tissue-reactive antibodies were markedly deposited in the damaged tissues (Figures 6B and 6C). These results indicate that CCR7- or CCR7L-deficient mice exhibit autoimmune exocrinopathy resembling Sjögren's syndrome.

To examine whether the autoimmune exocrinopathy is a direct consequence of the defect in thymocytes, the CCR7L-deficient *plt/plt* thymocytes were transferred into RAG2-deficient mice that lacked T cells and B cells. Under this experimental condition, the *plt/plt*

thymocytes were not defective in CCR7 expression, and the host RAG2-deficient mice were not defective in CCR7L expression. CCR7-expressing *plt/plt*-derived T cells would normally migrate to CCR7L-expressing host tissues, including lymph nodes and exocrine glands, in the RAG2-deficient mice. Thus, the defect in CCR7/CCR7L signaling in this cell transfer experiment would be limited to the period of thymocyte development before the cell transfer, and the transferred thymocyte-derived T cells would exhibit no or little aberrancy in the peripheral distribution after the cell transfer. As shown in Figures 7A and 7B, the transfer of CCR7L-deficient *plt/plt* thymocytes as well as *plt/plt* spleen cells caused significant lymphocyte infiltration in the lacrimal and salivary glands. By contrast, the transfer of control *+/plt* thymocytes or *+/plt* spleen cells did not cause such lymphocyte infiltration (Figures 7A and 7B). These results indicate that the thymocytes generated without CCR7L are potent in inducing autoimmune exocrinopathy in mice and, thus, are defective in establishing central tolerance.

It was previously shown that *plt/plt* or CCR7-deficient mice are defective in forming the medullary architecture characterized by clusters of UEA-1$^+$ cells (Ueno et al., 2004). We finally addressed whether the defective central tolerance in the thymus lacking CCR7 or CCR7L is due to defective thymocyte accumulation in the medulla or defective architecture of the medullary stroma. To this end, we generated mixed bone marrow chimeras reconstituted with equal numbers of bone marrow cells from CCR7-deficient mice and normal mice and examined whether these mixed bone marrow chimeras might exhibit the autoimmune exocrinopathy. Due to the presence of normal bone-marrow-derived thymocytes, it was presumed that the medullary architecture in the mixed bone marrow chimeras would appear normal even in the presence of CCR7-deficient thymocytes. Indeed, normal architecture of the medullary region containing the UEA-1$^+$ clusters was detected in the mixed bone marrow chimeras, which was similar to that in the normal bone marrow chimeras and different from that in CCR7-deficient bone marrow chimeras (Figure 7C), whereas the accumulation of CD45.2$^+$ CCR7-deficient thymocytes in the medulla was severely defective in the mixed bone marrow chimeras (Figure 7D). However, these mixed bone marrow chimeras exhibited the autoimmune phenotypes in the lacrimal glands, including lymphocyte infiltration and tissue damage, similar to the bone marrow chimeras reconstituted with CCR7-deficient bone marrow cells alone (Figures 7E and 7F). These results indicate that CCR7-deficient bone-marrow-derived cells that are reconstituted in the normal thymus architecture are potent in inducing autoimmune exocrinopathy, suggesting that the autoimmune phenotype in CCR7-deficient mice is likely due to the lack of thymocyte accumulation in the medulla rather than the defective development of the medullary architecture. These results also indicate that CCR7-deficient bone-marrow-derived cells that are reconstituted in the presence of normally developing hematopoietic cells are still potent in inducing autoimmune exocrinopathy, suggesting that the autoimmunity in these mutant mice may be caused even in the presence of normally generated immune cells, including regulatory T cells.

Discussion

The present results show that mature thymocytes are normally generated in developmental kinetics and are normally exported in CCR7- or CCR7L-deficient adult mice. The pharmacological inhibition of S1P-mediated thymocyte egress shows that in the absence of CCR7 signals, the mature thymocytes are accumulated in the thymic cortex rather than the thymic medulla, suggesting that the S1P-mediated thymocyte egress may occur in the thymic cortex of these mutant mice. These results argue the possibility that the thymic medulla may not be required for the maturation or export of thymocytes. On the other hand, our results also show that in the absence of CCR7 signals, the mature thymocytes are incapable of acquiring tolerance to lacrimal and salivary glands and are potent in inducing autoimmune exocrinopathy. Thus, CCR7-mediated cortex-to-medulla migration of positively selected thymocytes is essential for establishing central tolerance rather than for supporting the maturation or export of thymocytes.

The Cortex and Thymocyte Export

Our results show that the developmental kinetics and the thymic export of SP thymocytes are undisturbed in adult mice lacking CCR7 or CCR7L. FTY720 treatment shows that the mature thymocytes are accumulated in the thymic cortex of CCR7- or CCR7L-deficient mice, unlike the accumulation in the medulla of normal mice. FTY720-sensitive S1P-dependent chemotaxis is essential for the egress of mature thymocytes to the circulation (Matloubian et al., 2004). Thus, the present results suggest that the mature thymocytes generated in CCR7- or CCR7L-deficient mice may be exported from the cortex without migrating into the medulla. It has been generally thought that the medulla is a place for the maturation and export of thymocytes (Ritter and Boyd, 1993; Scollay and Godfrey, 1995; Anderson and Jenkinson, 2001). Indeed, our results from the FTY720 treatment of normal mice agree with the notion that S1P-dependent thymocyte export occurs in the medulla of normal mice (Figure 3). However, our results also suggest the possibility that in the case that the positively selected thymocytes remain in the cortex without being attracted to CCR7L expressed in the medulla, the thymic cortex can not only nurture the maturation of SP thymocytes but also export the mature thymocytes. Based on these results, we propose the possibility that the thymic cortex may have the capability of fully supporting the development of T cells, including SP thymocyte maturation and the export of mature T cells. This possibility is consistent with previous findings that T cell maturation and peripheral supply are not perturbed in relB-deficient mice that lack the thymic medulla (Burkly et al., 1995).

It should be noted that we detected a minor fraction of mature SP thymocytes in the medullary areas of CCR7- or CCR7L-deficient mice (Ueno et al., 2004). However, FTY720 treatment does not cause the accumulation of mature thymocytes in the medulla of CCR7- or CCR7L-deficient mice (Figure 3), arguing the possibility that those medullary thymocytes in CCR7- or CCR7L-deficient mice do not represent mature thymocytes whose S1P-dependent egress from the thymus is blocked. It is even unclear whether those medullary thymocytes in

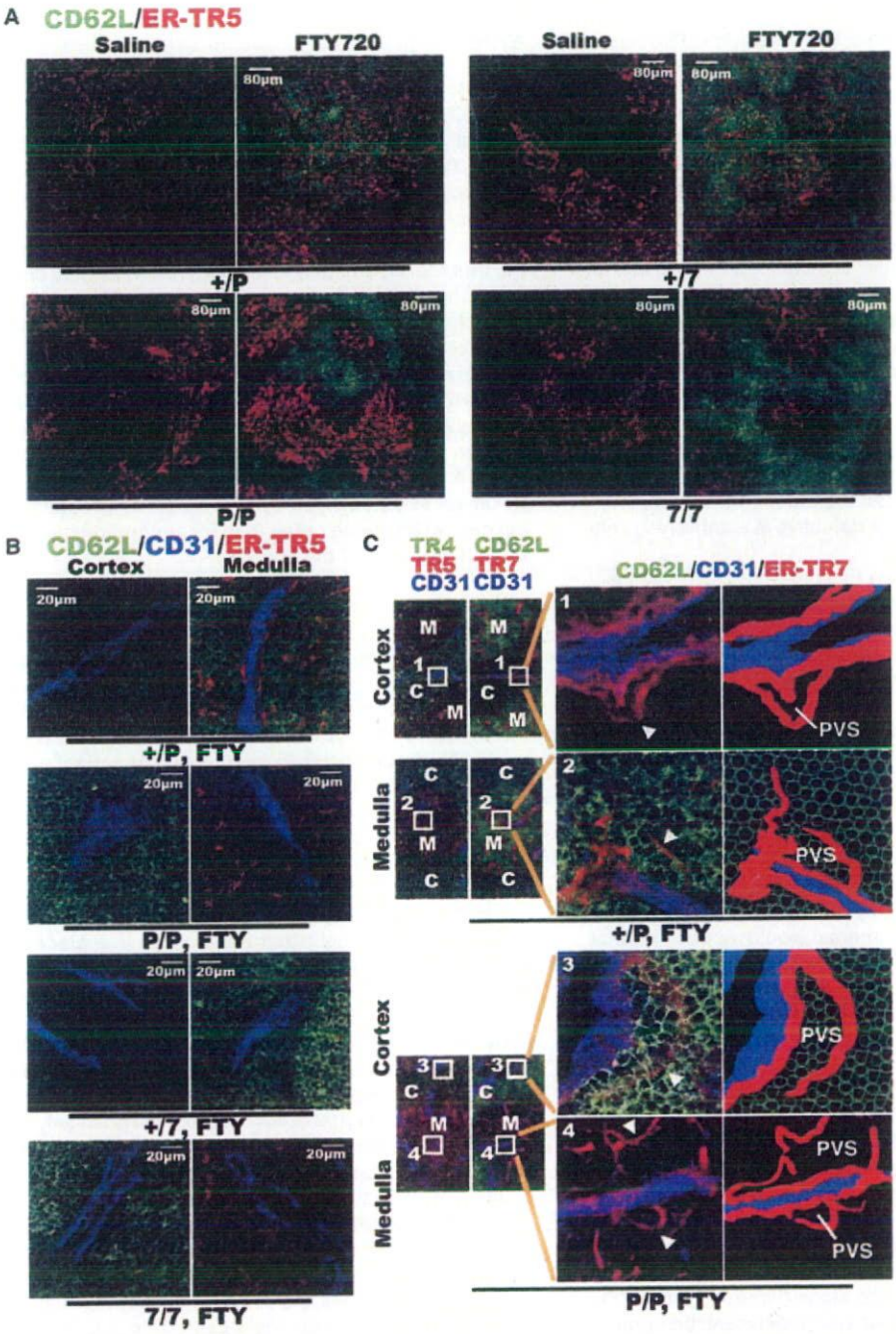

Figure 3. FTY720-Mediated Accumulation of Mature Thymocytes in the Thymic Cortex of CCR7- or CCR7L-Deficient Mice

Frozen sections of the thymus from indicated mice were two-color or three-color stained for CD62L (green) and mTEC-specific ER-TR5 (red) (A); CD62L (green), CD31 (blue), and ER-TR5 (red) (B); ER-TR4 (green), CD31 (blue), and ER-TR5 (red) (C); or CD62L (green), CD31 (blue), and ER-TR7 (red) (C), as indicated. The cortex and the medulla in (B) were identified by staining of the adjacent sections with cTEC-specific ER-TR4 and mTEC-specific ER-TR5. The high magnification images in (B) show that in the cortex of FTY720-mediated CCR7L-deficient mice (P/P) and CCR7-deficient mice (7/7) and in the medulla of FTY720-mediated control mice (+/P and +/7), there are the areas where many CD62L^{high} thymocytes were accumulated around CD31^{+} endothelial vessels. It should be noted that low-magnification images of the cortex in the FTY720-treated mutant mice (P/P and 7/7) and of the medulla in the FTY720-treated control mice (+/P and +/7) show that not all areas in the cortex are uniformly filled with CD62L^{high} thymocytes and that there are also the cortical areas where only a few CD62L^{high} thymocytes were found (A). On the other hand, no or very few CD62L^{high} thymocytes were found in the medulla of FTY720-mediated CCR7- or CCR7L-deficient mice (P/P and 7/7) and in the cortex of FTY720-mediated control mice (+/P and +/7) in low-magnification as well as in high-magnification images (A and B).

(C) Serial sections were stained as indicated. The cortex (C) and the medulla (M) were identified by ER-TR4 and ER-TR5. The perivascular space (PVS) was identified as the areas surrounded by CD31^{+} endothelial and ER-TR7^{+} mesenchymal cells. High-magnification images of boxes 1, 2, 3,

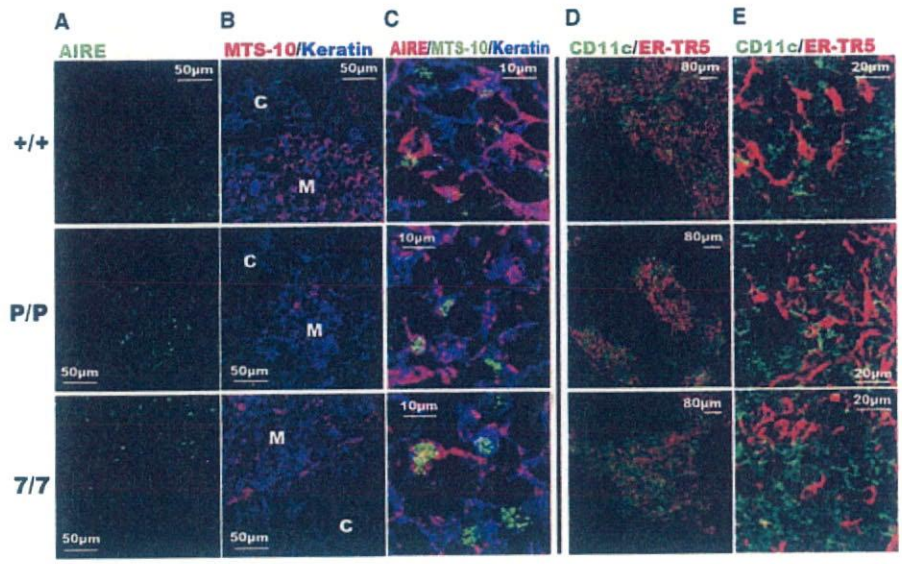

Figure 4. Intrathymic Distribution of AIRE-Expressing Cells and DCs in CCR7- or CCR7L-Deficient Mice

(A–C) Thymus sections from B6 (+/+), *plt/plt* (P/P), and CCR7-deficient (7/7) adult mice were stained with anti-AIRE (green), anti-keratin (blue), and mTEC-specific MTS-10 (red) antibodies. Cortex (C) and medulla (M) were identified with MTS-10 staining (B). High-magnification images from the three-color staining in (C) show that AIRE, keratin, and the MTS-10 determinant in the mutant mice as well as in the control mice are expressed in single mTEC, although AIRE is selectively localized in the nuclei whereas keratin and MTS-10 determinants are predominantly localized at the cytoplasm and the plasma membrane, respectively.

(D and E) Thymus sections from indicated mice were also stained for CD11c (green) and ER-TR5 (red).

Shown are representative results of more than three independent analyses.

the mutant mice may represent mature thymocytes that will eventually be exported from the thymus. Nevertheless, it is possible that some mature thymocytes in CCR7- or CCR7L-deficient mice may egress from the thymus through the medullary and/or cortico-medullary junction areas.

Perhaps, however, it is more tempting to speculate that the minor fraction of mature thymocytes found in the medulla of CCR7- or CCR7L-deficient mice may contribute to the crosstalk signals to induce the generation of AIRE$^+$ mTEC in the medullary area. It was previously shown that the generation of mature SP thymocytes is essential for the development of the medullary epithelial architecture (van Ewijk et al., 1994). On the other hand, CCR7- or CCR7L-deficient mice generate the thymus with a small but distinct medullary region (Ueno et al., 2004) that contains AIRE$^+$ mTEC as well as DCs (Figure 4), even though the generation of UEA-1$^+$ clusters in the medulla is impaired (Ueno et al., 2004; also shown in Figure 7 of this study). Thus, it is possible that the CCR7-independent migration into the medulla by a small fraction of mature thymocytes may play a role in the development of TEC precursor cells to generate AIRE$^+$ mTEC and the localization of DCs in the medulla.

The perivascular space in the postnatal thymus is distributed around the venules and some arterioles and is enriched in the medulla and the cortico-medullary junction (Ushiki, 1986; Kato, 1997). However, the perivascular space is also found within the cortex in normal animals (Ushiki, 1986; Kato, 1997; F.S. and Y.T., unpublished data). It has been speculated that the perivascular space is a route for T cell egress from the thymus parenchyma to the circulation (Ushiki, 1986; Kato, 1997). Indeed, our results show that the FTY720-mediated blockade of the S1P-dependent egress results in the accumulation of mature thymocytes even in the perivascular space that is localized in the medulla of normal mice (Figure 3C), supporting the possibility that the medullary perivascular space is a route for the S1P-dependent T cell egress from the thymus in normal mice. Interestingly, however, in mice deficient in CCR7 or CCR7L, the FTY720 treatment accumulates most mature thymocytes in the cortex rather than in the medulla. The accumulation in these mutant mice is detected even in the perivascular space within the cortex (Figure 3C). These results not only reinforce the possibility that the cortex is capable of supporting T cell export, but also support the possibility that the perivascular space within the cortex can serve as a route for the S1P-dependent egress of mature thymocytes. Thus, our results suggest that the cortex-to-medulla migration of developing thymocytes may not be required for the further maturation of thymocytes or for the export of mature thymocytes.

The possibility that similar to the medulla, the cortex can support the generation and export of mature SP thymocytes prompts us to question why the maturation

and 4 show the representative areas of cortical PVS in +/P mice, medullary PVS in +/P mice, cortical PVS in P/P mice, and medullary PVS in P/P mice, respectively. Arrows in the high-magnification images (1–4) indicate the representative PVSs, which are also schematically depicted in the right panels. Shown are representative results of more than ten independent analyses.

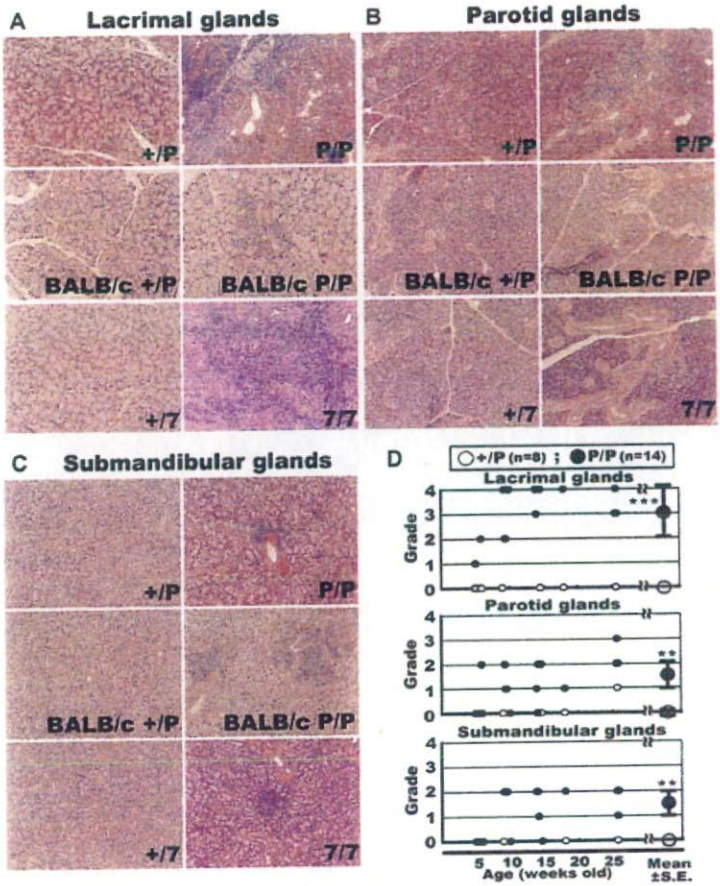

Figure 5. CCR7- or CCR7L-Deficient Mice Exhibit Lymphocyte Infiltration in Lacrimal and Salivary Glands with Tissue Damage

Representative hematoxylin- and eosin-stained tissue sections of lacrimal glands (A), parotid glands (B), and submandibular glands (C) from CCR7L-deficient mice (*plt/plt*, P/P), CCR7-deficient mice (7/7), and their heterozygous control mice (+/P and +/7) are shown. Where indicated, the sections were obtained from *plt/plt* (P/P) and +/*plt* (+/P) mice of BALB/c background.

(D) Histological grading of inflammatory lesions in *plt/plt* (P/P; closed circles) and +/*plt* (+/P; open circles) mice at the indicated age was performed as described in the Experimental Procedures. Double asterisk indicates $p < 0.005$ and triple asterisk indicates $p < 0.0005$ by the Mann-Whitney test.

and export of SP thymocytes in normal mice occur predominantly in the medulla rather than in the cortex. In agreement with previous reports (Matloubian et al., 2004; Allende et al., 2004), our results show that S1P1, the receptor for S1P in T cells, is expressed predominantly by $CD62L^{high}CD69^{low}$ mature SP thymocytes rather than by the less immature thymocytes, including DN, DP, and $CD62L^{low}CD69^{high}$ SP cells. It is therefore likely that most thymocytes, including the DN and DP immature cortical thymocytes as well as the $CD62L^{low}CD69^{high}$ semimature SP thymocytes, are not attracted to S1P, even though neighboring vasculatures in the cortex may supply a gradient of S1P toward the circulation. On the other hand, positively selected DP thymocytes begin expressing a low level of CCR7 (Ueno et al., 2004), and CCR7 is clearly expressed on the positively selected thymocytes at the semimature $CD62L^{low}CD69^{high}$ SP thymocyte stage (Figure 1). Thus, it is likely that in normal mice, positively selected thymocytes in the cortex are attracted to CCR7L, which is predominantly expressed in the medulla, but not attracted to S1P, which penetrates from the vasculature even in the cortex, so that the majority of the positively selected thymocytes are attracted to and accumulated in the medulla. Upon completion of thymocyte differentiation, the S1P1-expressing mature SP thymocytes may be exported to the circulation via the perivascular space within either the medulla or the cortex.

It is also interesting to note that $CD62L^{+}$ cells are sparsely found in the cortex, rather than in the medulla, of the normal untreated mice (Figure 3A), in agreement with previous reports (Reichert et al., 1984; Fink et al., 1985). It was reported that $CD62L^{+}$ cortical thymocytes in normal untreated mice are generated before birth and contain immature DN cells (Reichert et al., 1986a, 1986b), whereas $CD62L^{high}$ mature SP thymocytes are rare in untreated mice and are increased in number upon FTY720 treatment within the medulla of normal mice (Figures 2C and 3A). The developmental status, particularly the significance in thymocyte export, of the $CD62L^{+}$ cells visualized in the cortex of normal untreated mice is still unclear and warrants further analysis.

Medulla Migration and Central Tolerance

Our results show that CCR7- or CCR7L-deficient mice exhibit autoimmune dacryoadenitis and sialadenitis with antibody deposit and tissue damage and that this exocrinopathy is reproduced in lymphocyte-lacking RAG2-deficient mice that are transferred with thymocytes from CCR7L-deficient mice. These results indicate that the thymocytes that are generated without CCR7 signals do not fully establish self-tolerance to the organs, such as lacrimal and salivary glands. Because thymocytes that develop in CCR7- or CCR7L-deficient mice fail to accumulate in the medulla and may be exported directly from the cortex, and because $AIRE^{+}$ cells in the

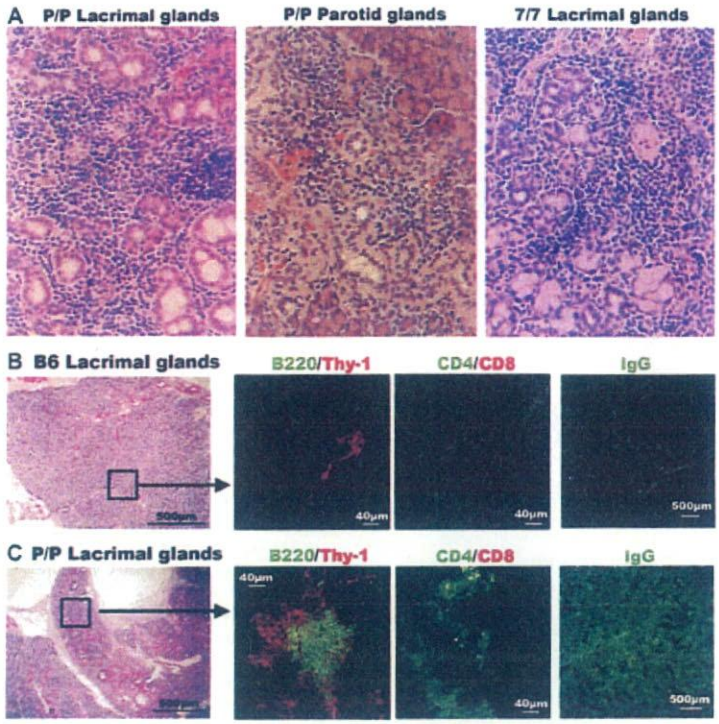

Figure 6. CCR7- or CCR7L-Deficient Mice Exhibit Autoimmune Exocrinopathy

(A) Representative sections of indicated exocrine glands from CCR7L-deficient *plt/plt* mice (P/P) and CCR7-deficient mice (7/7) show that acinar cells in the lacrimal and parotid glands are definitively destoyed in the mutant mice, presenting clear evidence of tissue damage in the mutant mice.

(B and C) Serial sections of lacrimal glands from B6 mice (B) and CCR7L-deficient *plt/plt* mice (P/P) (C) were stained with hematoxylin and eosin or with indicated antibodies. Antibodies used were specific for B220 (green), Thy-1 (red), CD4 (green), CD8 (red), and IgG (green). Shown are representative results of four independent analyses.

thymus are predominantly confined within the medulla even in CCR7- or CCR7L-deficient mice, it is possible that the thymocytes generated in CCR7- or CCR7L-deficient mice are unable to establish self-tolerance to a spectrum of organ-specific antigens because the developing thymocytes fail to interact with AIRE$^+$ mTEC localized in the medulla.

It is interesting to note that similar to CCR7- or CCR7L-deficient mice, AIRE-deficient mice as well as AIRE-deficient APECED patients manifest autoimmune dacryoadenitis and sialadenitis (Anderson et al., 2002; Liston et al., 2003; Kuroda et al., 2005), suggesting that a similar mechanism for the breakdown of central tolerance may be involved in the autoimmunity in these cases. The autoimmune phenotype in CCR7- or CCR7L-deficient mice is mild and restricted to lacrimal and salivary glands. It has been reported that the autoimmune phenotype in AIRE-deficient mice of C57BL/6 background is also mild, being largely limited to lacrimal and salivary glands (Jiang et al., 2005; Kuroda et al., 2005). Thus, the autoimmune phenotype in CCR7- or CCR7L-deficient mice and in AIRE-deficient mice is similarly mild and similarly restricted to lacrimal and salivary glands, at least in the C57BL/6 background. Whether or not the autoimmune phenotype in CCR7- or CCR7L-deficient mice of other genetic backgrounds, particularly the autoimmune-prone NOD background, may be broader and more severe, similar to the phenotype of AIRE-deficient mice, is still unclear and will be addressed in a separate study.

Nonetheless, AIRE-deficient mice of different genetic backgrounds as well as many APECED patients manifest autoimmunity with a spectrum that appears much wider than dacryoadenitis and sialadenitis in CCR7- or CCR7L-deficient mice of the C57BL/6 background (Nagamine et al., 1997; Aaltonen et al., 1997; Anderson et al., 2002; Jiang et al., 2005). It was recently shown that central tolerance to organ-specific antigens is induced not only directly by mTEC antigen presentation but also indirectly by bone-marrow-derived antigen-presenting cells such as DCs (Gallegos and Bevan, 2004). Our results show that DCs in the thymus of CCR7- or CCR7L-deficient mice are normally distributed in the cortex as well as in the medulla (Figure 4). Thus, the more restricted autoimmunity in CCR7- or CCR7L-deficient mice may be due at least in part to central tolerance to DC-mediated crosspresentation of a fraction of AIRE-dependent, organ-specific antigens expressed by mTEC. The milder autoimmunity in CCR7- or CCR7L-deficient mice than in AIRE-deficient mice may also be affected by the compromised immune responses in CCR7- or CCR7L-deficient mice, which are caused by the delayed lymphocyte homing to secondary lymphoid organs (Forster et al., 1999), even though our results show that the similarly mild autoimmune exocrinopathy is caused even in RAG2-deficient mice reconstituted with *plt/plt* thymocytes (Figure 7) in which CCR7/CCR7L signaling in peripheral mature T cells would exhibit no or little aberrancy. How the autoimmunity in CCR7-, CCR7L-, or AIRE-deficient mice is limited to dacryoadenitis and sialadenitis in the C57BL/6 background is still unclear.

We think it is possible that the clonal deletion of self-reactive thymocytes that are specific for a spectrum of organ-specific antigens may be affected in CCR7- or CCR7L-deficient mice, because the thymocytes from these mutant mice exhibit a significantly higher autologous mixed lymphocyte reaction than those from

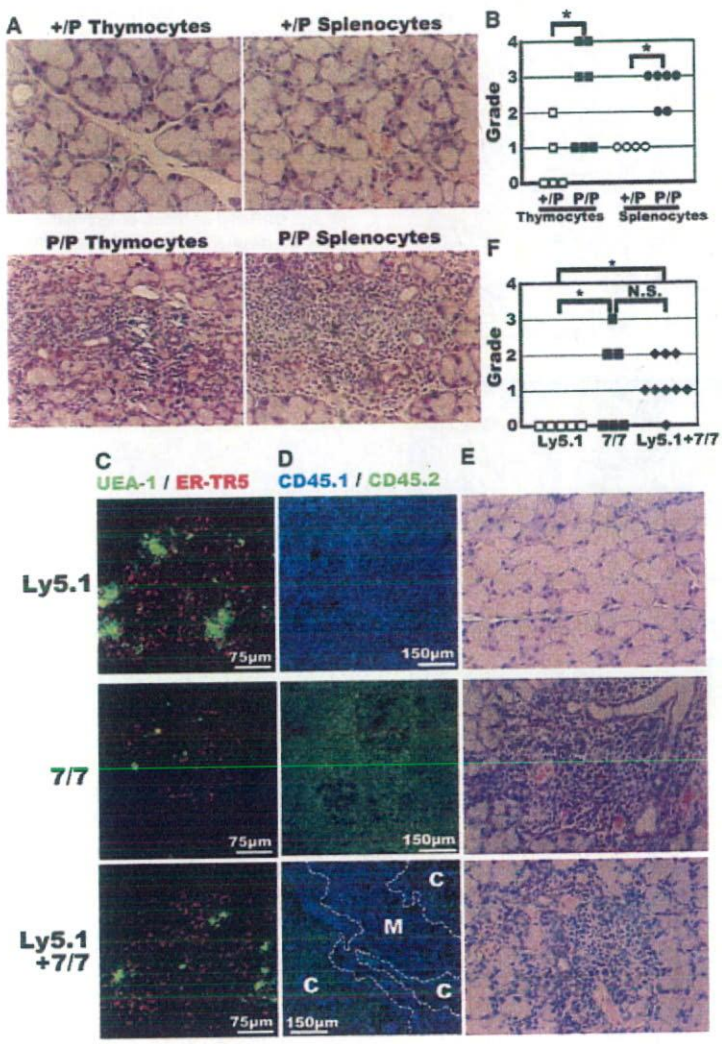

Figure 7. Exocrinopathy Is Associated with Defective Medulla Accumulation of Thymocytes

(A and B) Thymocytes generated in CCR7L-deficient mice are potent in inducing dacryoadenitis and sialadenitis. Thymocytes and splenocytes from CCR7L-deficient *plt/plt* mice (P/P) or control *+/plt* mice were transferred into nonirradiated RAG2-deficient mice. Histopathological analysis was carried out 6 weeks after the cell transfer. Tissue sections of lacrimal glands were stained with hematoxylin and eosin (A), and histological grading was performed as described in the Experimental Procedures (B).

(C–F) T cell-depleted bone marrow cells from B6.SJL-Pt_{prc} mice (Ly5.1; $CD45.1^+CD45.2^-$) and/or CCR7-deficient mice (7/7; $CD45.1^-CD45.2^+$) were transferred into nonirradiated RAG2-deficient mice. Where indicated, equal numbers of T cell-depleted bone marrow cells from B6.SJL-Pt_{prc} mice and CCR7-deficient mice were transferred (Ly5.1+7.7). Histological and flow cytometry analyses were carried out 6–8 weeks after the cell transfer. The thymuses were analyzed with multicolor confocal microscopy (C) and flow cytometry (data not shown). The UEA-1 and ER-TR5 two-color staining profiles indicate that clusters of $UEA\text{-}1^+$ cells in the medulla are generated in the B6.SJL-Pt_{prc} bone marrow chimeras (Ly5.1) and the mixed bone marrow chimeras (Ly5.1+7/7) but are defective in the CCR7-deficient bone marrow chimeras (7/7) (C). Flow cytometry analysis indicated that every mouse used for the analysis exhibited successful thymocyte reconstitution ($2.0–2.5 \times 10^8$ cells per mouse) and that the ratio of $CD45.1^+CD45.2^-$ thymocytes to $CD45.1^-CD45.2^+$ thymocytes in the mixed bone marrow chimeras was in the range of 40:60 to 60:40 (data not shown). The CD45.2 and CD45.1 two-color confocal analysis of the thymus sections (D) along with the staining of the adjacent sections with mTEC-specific ER-TR5 and UEA-1 indicates that $CD45.1^-CD45.2^+$ CCR7-deficient thymocytes are arrested in the cortex (C) and are defective in accumulating in the medulla (M) of the mixed bone marrow chimeras. Tissue sections of lacrimal glands were stained with hematoxylin and eosin (E), and histological grading was performed as described in the Experimental Procedures (F). Asterisk indicates $p < 0.05$ by the Mann-Whitney test; N.S., not significant.

normal mice (H.K. and Y.T., unpublished data), because the mixed bone marrow chimeras reconstituted with bone marrow cells from CCR7-deficient mice and normal mice exhibit the autoimmune exocrinopathy (Figure 7) and because AIRE-expressing mTEC are shown to regulate the deletion of forbidden thymocyte clones (Liston et al., 2003) rather than the generation of regulatory T cells (Anderson et al., 2005). We are currently analyzing whether the clonal deletion of organ-specific-antigen-reactive thymocytes and/or the generation of regulatory T cells may be defective in the thymus of CCR7- or CCR7L-deficient mice.

We have previously reported that negative selection is normally induced in male antigen-specific thymocytes in HY-TCR-transgenic mice and in allogeneic MHC-specific thymocytes in 2C-TCR-transgenic mice even in the absence of CCR7L (Ueno et al., 2004), indicating that negative selection to systemically ubiquitous antigens is normally induced in the absence of CCR7 signals. Perhaps, negative selection to ubiquitous antigens occurs in the cortex without migration to the medulla. We have also shown that Mtv-specific deletion of $V\beta3^+$ and $V\beta5^+$ thymocytes is normally induced in CCR7L-deficient mice (Ueno et al., 2004). It has been reported that DCs in the thymus are primarily responsible for negative selection of Mtv-reactive thymocytes (Moore et al., 1994; Ferrero et al., 1997). Our results show that in CCR7- or CCR7L-deficient mice as well as in normal

mice, DCs are localized mostly in the medulla and sparsely in the cortex. Thus, it is possible that the sparsely localized DCs in the cortex may be capable of inducing negative selection of Mtv-reactive thymocytes in the absence of CCR7 signals and without the medulla migration. The average lifespan of SP thymocytes in the thymus is 12 days (Egerton et al., 1990; Scollay and Godfrey, 1995), and the developmental kinetics of the SP thymocytes is undisturbed in the absence of CCR7 signals (Figure 1); thus, 12 days in the cortex may be sufficient for developing SP thymocytes to be negatively selected with Mtv-superantigens presented by DCs.

In conclusion, the present results indicate that the CCR7-dependent accumulation of positively selected thymocytes in the medulla is not essential for the maturation or export of thymocytes, suggesting that similar to the medulla, the thymic cortex may be capable of supporting the development and export of mature thymocytes. On the other hand, the cortex-to-medulla migration of developing thymocytes is essential for establishing central tolerance, suggesting that the developing thymocytes need to directly interact with mTEC in order to establish central tolerance to some organ-specific antigens.

Experimental Procedures

Mice

CCR7-deficient mice (Forster et al., 1999) and CCR7L-deficient *plt/plt* mice (Nakano et al., 1998) were backcrossed to C57BL/6 mice for six generations. *plt/plt* mice of BALB/c background were also used. RAG2-deficient mice and B6.SJL-Pt_{prc} mice were kindly provided by Dr. F. Alt (Shinkai et al., 1993) and Dr. H. Nakauchi, respectively. C57BL/6 (B6) mice were obtained from SLC, Shizuoka, Japan. Mice were bred and maintained under specific pathogen-free conditions in our animal facility, and experiments were performed with consent from the Animal Experimentation Committee of the University of Tokushima.

BrdU Labeling

For the detection of BrdU incorporation, adult mice were injected intraperitoneally twice with 2 mg BrdU/mouse at 4 hr intervals. Thymocytes were harvested at indicated time points after the injection. Cells that incorporated BrdU were detected with an FITC BrdU Flow Kit according to the manufacturer's instructions (BD Biosciences).

FTY720 Treatment

FTY720 (Novartis Pharma) was dissolved in saline and administered into the peritoneal cavity of adult mice at the dose of 20 μg per day for 10 days. Mice were analyzed on the day after the last administration.

Cell Transfer into RAG2-Deficient Mice

Thymocytes, splenocytes, or T cell-depleted bone marrow cells from female mice (3×10^7) were injected intravenously into nonirradiated RAG2-deficient female mice. Mice were analyzed 6–8 weeks after the cell transfer.

Multicolor Confocal Analysis

Frozen sections (5–10 μm) were fixed with acetone and stained with the following antibodies: Alexa 488-conjugated anti-CD4 (GK1.5), FITC-conjugated anti-B220 (RA3-6B2), Alexa 633-conjugated mTEC-specific ER-TR5 (van Vliet et al., 1984), and Alexa 633-conjugated anti-mouse IgG antibodies. Alexa 546-conjugated UEA-1 was also used. Biotinylated antibodies specific for CD8 (53-6-72), CD11c (HL-3), CD31 (clone 390), Thy1.2 (30-H12), and CD45.2 (clone 104) were visualized with Alexa 488-, Alexa 568-, or Alexa 633-conjugated streptavidin (Molecular Probes). The staining with anti-CD62L (MEL-14), cTEC-specific ER-TR4 (van Vliet et al., 1984), and fibroblast-specific ER-TR7 (van Vliet et al., 1984) was visualized with Alexa 488- or Alexa 633-conjugated anti-rat IgG (Molecular Probes). The staining with anti-CD45.1 antibody (clone A20) was visualized with Alexa 633-conjugated anti-mouse IgG (Molecular Probes). The images were acquired with a TCS SP2 confocal laser-scanning microscope (Leica) equipped with Ar and He-Ne lasers (excitations at 488, 568, and 633 nm) and analyzed with Leica Confocal software version 2.6.

Where indicated, frozen sections were labeled with rabbit anti-mouse pan-cytokeratin antibody (wide screen, Dako), mTEC-specific MTS-10 (Godfrey et al., 1990), and anti-AIRE antibody (clone 5H12) (Liston et al., 2004) followed by Alexa 647-conjugated anti-rabbit IgG (Molecular Probes), biotinylated anti-rat IgM (Southern Biotech), and FITC-labeled anti-rat IgG2c (Southern Biotech) antibodies. Biotinylated antibody was visualized with Alexa 568-conjugated streptavidin. The confocal images were acquired with a Bio-Rad MRC 1024 with a three-line Kr/Ag laser (excitations at 488, 568, and 647 nm) and were analyzed with Bio-Rad LaserSharp software version 3.2.

Histopathology

Paraformaldehyde-fixed tissues were embedded in paraffin. The sections (4 μm) were stained with hematoxylin and eosin. Histological grading of inflammatory lesions was carried out according to the method originally reported by White and Casarett (1974) as follows (Ishimaru et al., 2000): a score of 1 indicates that one to five foci being composed of more than 20 mononuclear cells per focus were seen; a score of 2 indicates that more than five such foci were seen but without significant parenchymal damage; a score of 3 indicates degeneration of parenchymal tissue; and a score of 4 indicates extensive infiltration of the glands with mononuclear cells and extensive parenchymal damage.

Multicolor Flow Cytometry Analysis

Single-cell suspensions were stained with FITC-labeled, PE-labeled, APC-labeled, and/or biotinylated antibodies as described (Ueno et al., 2002, 2004). Biotinylated antibodies were detected with PE- or APC-conjugated streptavidin (Molecular Probes) or Cy7-APC-conjugated streptavidin (Caltag Laboratories). Labeled monoclonal antibodies and normal IgG controls were obtained from BD Biosciences and eBiosciences. Staining with CCL19-Ig (a gift from Dr. Kunio Hieshima) was visualized with biotinylated anti-human IgG and APC-conjugated streptavidin (Ueno et al., 2004). Multicolor flow cytometry analysis was performed with two-laser FACS-Calibur or FACS-Vantage (Becton Dickinson). Data were obtained with Cell Quest software for viable cells that were determined based on measurements of forward light scatter intensity and propidium iodide exclusion.

Quantitative RT-PCR Analysis

Total cellular RNA was reverse-transcribed by using SuperScript II Reverse Transcriptase (Life Technologies) and oligo-dT oligonucleotide. cDNA was polymerase chain reaction (PCR) amplified with a SYBR Green PCR Master Mix and an ABI PRISM Sequence Detection System (Applied Biosystems) for CCR7 (5′-TGTACGTCAGTA TCACCAGC-3′ and 5′-TTTTCCAGGTGTGCTTCTGC-3′), S1P1 (5′-GTGTAGACCCAGAGTCCTGCG-3′ and 5′-AGCTTTTCCTTGGCTG GAGAG-3′), and GAPDH (5′-CCGGTGCTGAGTATGTCGTG-3′ and 5′-CAGTCTTCTGGGTGGCAGTG-3′). Amplified signals were confirmed to be single bands by using gel electrophoresis and were normalized to GAPDH levels.

Acknowledgments

We thank Drs. Hamish Scott and Daniel Gray for AIRE expression analysis; Drs. Hideki Nakano and Terutaka Kakiuchi for *plt/plt* mice; Dr. Fred Alt for RAG2-knockout mice; Dr. Willem van Ewijk for ER-TR monoclonal antibodies; Dr. Kunio Hieshima for CCL19-Ig; Drs. Takeshi Nitta and Norimasa Iwanami for reading the manuscript; and Novartis Pharma for FTY720. This work was supported by Grants-in-Aid for Scientific Research from the MEXT and JSPS, the JSPS Core-to-Core Program, and the JSPS Center of Excellence Program, and the University of Tokushima pilot research program.

Received: June 23, 2005
Revised: October 31, 2005
Accepted: December 27, 2005
Published: February 14, 2006

References

Aaltonen, J., Bjorses, P., Perheentupa, J., Horelli-Kuitunen, N., Palotie, A., Peltonen, L., Lee, Y.S., Francis, F., Henning, S., Thiel, C., et al. (1997). An autoimmune disease, APECED, caused by mutations in a novel gene featuring two PHD-type zinc-finger domains. Nat. Genet. *17*, 399–403.

Akiyama, T., Maeda, S., Yamane, S., Ogino, K., Kasai, M., Kajiura, F., Matsumoto, M., and Inoue, J. (2005). Dependence of self-tolerance on TRAF6-directed development of thymic stroma. Science *308*, 248–251.

Allende, M.L., Dreier, J.L., Mandala, S., and Proia, R.L. (2004). Expression of the sphingosine 1-phosphate receptor, S1P1, on T-cells controls thymic emigration. J. Biol. Chem. *279*, 15396–15401.

Anderson, G., and Jenkinson, E.J. (2001). Lymphostromal interactions in thymic development and function. Nat. Rev. Immunol. *1*, 31–40.

Anderson, M.S., Venanzi, E.S., Klein, L., Chen, Z., Berzins, S.P., Turley, S.J., von Boehmer, H., Bronson, R., Dierich, A., Benoist, C., and Mathis, D. (2002). Projection of an immunological self shadow within the thymus by the aire protein. Science *298*, 1395–1401.

Anderson, M.S., Venanzi, E.S., Chen, Z., Berzins, S.P., Benoist, C., and Mathis, D. (2005). The cellular mechanism of Aire control of T cell tolerance. Immunity *23*, 227–239.

Benz, C., Heinzel, K., and Bleul, C.C. (2004). Homing of immature thymocytes to the subcapsular microenvironment within the thymus is not an absolute requirement for T cell development. Eur. J. Immunol. *34*, 3652–3663.

Bjorses, P., Pelto-Huikko, M., Kaukonen, J., Aaltonen, J., Peltonen, L., and Ulmanen, I. (1999). Localization of the APECED protein in distinct nuclear structures. Hum. Mol. Genet. *8*, 259–266.

Blackburn, C.C., Manley, N.R., Palmer, D.B., Boyd, R.L., Anderson, G., and Ritter, M.A. (2002). One for all and all for one: thymic epithelial stem cells and regeneration. Trends Immunol. *23*, 391–395.

Bleul, C.C., and Boehm, T. (2000). Chemokines define distinct microenvironments in the developing thymus. Eur. J. Immunol. *30*, 3371–3379.

Boehm, T., Scheu, S., Pfeffer, K., and Bleul, C.C. (2003). Thymic medullary epithelial cell differentiation, thymocyte emigration, and the control of autoimmunity require lympho-epithelial cross talk via LTβR. J. Exp. Med. *198*, 757–769.

Bousso, P., Bhakta, N.R., Lewis, R.S., and Robey, E. (2002). Dynamics of thymocyte-stromal cell interactions visualized by two-photon microscopy. Science *296*, 1876–1880.

Brinkmann, V., Davis, M.D., Heise, C.E., Albert, R., Cottens, S., Hof, R., Bruns, C., Prieschl, E., Baumruker, T., Hiestand, P., et al. (2002). The immune modulator FTY720 targets sphingosine 1-phosphate receptors. J. Biol. Chem. *277*, 21453–21457.

Burkly, L., Hession, C., Ogata, L., Reilly, C., Marconi, L.A., Olson, D., Tizard, R., Cate, R., and Lo, D. (1995). Expression of relB is required for the development of thymic medulla and dendritic cells. Nature *373*, 531–536.

Campbell, J.J., Pan, J., and Butcher, E.C. (1999). Developmental switches in chemokine responses during T cell maturation. J. Immunol. *163*, 2353–2357.

Chiba, K., Yanagawa, Y., Masubuchi, Y., Kataoka, H., Kawaguchi, T., Ohtsuki, M., and Hoshino, Y. (1998). FTY720, a novel immunosuppressant, induces sequestration of circulating mature lymphocytes by acceleration of lymphocyte homing in rats. I. FTY720 selectively decreases the number of circulating mature lymphocytes by acceleration of lymphocyte homing. J. Immunol. *160*, 5037–5044.

Egerton, M., Scollay, R., and Shortman, K. (1990). Kinetics of mature T-cell development in the thymus. Proc. Natl. Acad. Sci. USA *87*, 2579–2582.

Fairchild, P.J., and Austyn, J.M. (1990). Thymic dendritic cells: phenotype and function. Int. Rev. Immunol. *6*, 187–196.

Farr, A.G., Dooley, J.L., and Erickson, M. (2002). Organization of thymic medullary epithelial heterogeneity: implications for mechanisms of epithelial differentiation. Immunol. Rev. *189*, 20–27.

Ferrero, I., Anjuere, F., MacDonald, H.R., and Ardavin, C. (1997). In vitro negative selection of viral superantigen-reactive thymocytes by thymic dendritic cells. Blood *90*, 1943–1951.

Fink, P.J., Gallatin, W.M., Reichert, R.A., Butcher, E.C., and Weissman, I.L. (1985). Homing receptor-bearing thymocytes, an immunocompetent cortical subpopulation. Nature *313*, 233–235.

Flotte, T.J., Springer, T.A., and Thorbecke, G.J. (1983). Dendritic cell and macrophage staining by monoclonal antibodies in tissue sections and epidermal sheets. Am. J. Pathol. *111*, 112–124.

Forster, R., Schubel, A., Breitfeld, D., Kremmer, E., Renner-Muller, I., Wolf, E., and Lipp, M. (1999). CCR7 coordinates the primary immune response by establishing functional microenvironments in secondary lymphoid organs. Cell *99*, 23–33.

Gabor, M.J., Godfrey, D.I., and Scollay, R. (1997). Recent thymic emigrants are distinct from most medullary thymocytes. Eur. J. Immunol. *27*, 2010–2015.

Gallegos, A.M., and Bevan, M.J. (2004). Central tolerance to tissue-specific antigens mediated by direct and indirect antigen presentation. J. Exp. Med. *200*, 1039–1049.

Godfrey, D.I., Izon, D.J., Tucek, C.L., Wilson, T.J., and Boyd, R.L. (1990). The phenotypic heterogeneity of mouse thymic stromal cells. Immunology *70*, 66–74.

Gotter, J., and Kyewski, B. (2004). Regulating self-tolerance by deregulating gene expression. Curr. Opin. Immunol. *16*, 741–745.

Gray, D.H., Ueno, T., Chidgey, A.P., Malin, M., Goldberg, G.L., Takahama, Y., and Boyd, R.L. (2005). Controlling the thymic microenvironment. Curr. Opin. Immunol. *17*, 137–143.

Ishimaru, N., Yoneda, T., Saegusa, K., Yanagi, K., Haneji, N., Moriyama, K., Saito, I., and Hayashi, Y. (2000). Severe destructive autoimmune lesions with aging in murine Sjogren's syndrome through Fas-mediated apoptosis. Am. J. Pathol. *156*, 1557–1564.

Jiang, W., Anderson, M.S., Bronson, R., Mathis, D., and Benoist, C. (2005). Modifier loci condition autoimmunity provoked by Aire deficiency. J. Exp. Med. *202*, 805–815.

Kajiura, F., Sun, S., Nomura, T., Izumi, K., Ueno, T., Bando, Y., Kuroda, N., Han, H., Li, Y., Matsushima, A., et al. (2004). NF-κB-inducing kinase establishes self-tolerance in a thymic-stroma dependent manner. J. Immunol. *172*, 2067–2075.

Kato, S. (1997). Thymic microvascular system. Microsc. Res. Tech. *38*, 287–299.

Kim, C.H., Pelus, L.M., White, J.R., and Broxmeyer, H.E. (1998). Differential chemotactic behavior of developing T cells in response to thymic chemokines. Blood *91*, 4434–4443.

Kishimoto, H., and Sprent, J. (1997). Negative selection in the thymus includes semimature T cells. J. Exp. Med. *185*, 263–271.

Kuroda, N., Mitani, T., Takeda, N., Ishimaru, N., Arakaki, R., Hayashi, Y., Bando, Y., Izumi, K., Takahashi, T., Nomura, T., et al. (2005). Development of autoimmunity against transcriptionally unrepressed target antigen in the thymus of Aire-deficient mice. J. Immunol. *174*, 1862–1870.

Kwan, J., and Killeen, N. (2004). CCR7 directs the migration of thymocytes into the thymic medulla. J. Immunol. *172*, 3999–4007.

Lind, E.F., Prockop, S.E., Porritt, H.E., and Petrie, H.T. (2001). Mapping precursor movement through the postnatal thymus reveals specific microenvironments supporting defined stages of early lymphoid development. J. Exp. Med. *194*, 127–134.

Liston, A., Lesage, S., Wilson, J., Peltonen, L., and Goodnow, C.C. (2003). Aire regulates negative selection of organ-specific T cells. Nat. Immunol. *4*, 350–354.

Liston, A., Gray, D.H., Lesage, S., Fletcher, A.L., Wilson, J., Webster, K.E., Scott, H.S., Boyd, R.L., Peltonen, L., and Goodnow, C.C. (2004). Gene dosage—limiting role of Aire in thymic expression, clonal deletion, and organ-specific autoimmunity. J. Exp. Med. *200*, 1015–1026.

Liu, C., Ueno, T., Kuse, S., Saito, F., Nitta, T., Piali, L., Nakano, H., Kakiuchi, T., Lipp, M., Hollander, G.A., and Takahama, Y. (2005). The role of CCL21 in recruitment of T-precursor cells to fetal thymi. Blood *105*, 31–39.

Matloubian, M., Lo, C.G., Cinamon, G., Lesneski, M.J., Xu, Y., Brinkmann, V., Allende, M.L., Proia, R.L., and Cyster, J.G. (2004). Lymphocyte egress from thymus and peripheral lymphoid organs is dependent on S1P receptor 1. Nature *427*, 355–360.

Miller, J.F.A.P. (1961). Immunological function of the thymus. Lancet *2*, 748–749.

Misslitz, A., Pabst, O., Hintzen, G., Ohl, L., Kremmer, E., Petrie, H.T., and Forster, R. (2004). Thymic T cell development and progenitor localization depend on CCR7. J. Exp. Med. *200*, 481–491.

Moore, N.C., Anderson, G., McLoughlin, D.E., Owen, J.J., and Jenkinson, E.J. (1994). Differential expression of Mtv loci in MHC class II-positive thymic stromal cells. J. Immunol. *152*, 4826–4831.

Nagamine, K., Peterson, P., Scott, H.S., Kudoh, J., Minoshima, S., Heino, M., Krohn, K.J., Lalioti, M.D., Mullis, P.E., Antonarakis, S.E., et al. (1997). Positional cloning of the APECED gene. Nat. Genet. *17*, 393–398.

Nakano, H., Mori, S., Yonekawa, H., Nariuchi, H., Matsuzawa, A., and Kakiuchi, T. (1998). A novel mutant gene involved in T-lymphocyte-specific homing into peripheral lymphoid organs on mouse chromosome 4. Blood *91*, 2886–2895.

Palmer, E. (2003). Negative selection—clearing out the bad apples from the T-cell repertoire. Nat. Rev. Immunol. *3*, 383–391.

Plotkin, J., Prockop, S.E., Lepique, A., and Petrie, H.T. (2003). Critical role for CXCR4 signaling in progenitor localization and T cell differentiation in the postnatal thymus. J. Immunol. *171*, 4521–4527.

Ramsdell, F., Jenkins, M., Dinh, Q., and Fowlkes, B.J. (1991). The majority of CD4+8-thymocytes are functionally immature. J. Immunol. *147*, 1779–1785.

Reichert, R.A., Gallatin, W.M., Butcher, E.C., and Weissman, I.L. (1984). A homing receptor-bearing cortical thymocyte subset: implications for thymus cell migration and the nature of cortisone-resistant thymocytes. Cell *38*, 89–99.

Reichert, R.A., Weissman, I.L., and Butcher, E.C. (1986a). Phenotypic analysis of thymocytes that express homing receptors for peripheral lymph nodes. J. Immunol. *136*, 3521–3528.

Reichert, R.A., Jerabek, L., Gallatin, W.M., Butcher, E.C., and Weissman, I.L. (1986b). Ontogeny of lymphocyte homing receptor expression in the mouse thymus. J. Immunol. *136*, 3535–3542.

Rinderle, C., Christensen, H.M., Schweiger, S., Lehrach, H., and Yaspo, M.L. (1999). AIRE encodes a nuclear protein co-localizing with cytoskeletal filaments: altered sub-cellular distribution of mutants lacking the PHD zinc fingers. Hum. Mol. Genet. *8*, 277–290.

Ritter, M.A., and Boyd, R.L. (1993). Development in the thymus: it takes two to tango. Immunol. Today *14*, 462–469.

Scollay, R., and Godfrey, D.I. (1995). Thymic emigration: conveyor belts or lucky dips? Immunol. Today *16*, 268–274.

Sheard, M.A., Liu, C., and Takahama, Y. (2004). Developmental status of CD4–CD8$^+$ and CD4+CD8$^-$ thymocytes with medium expression of CD3. Eur. J. Immunol. *34*, 25–35.

Shinkai, Y., Koyasu, S., Nakayama, K., Murphy, K.M., Loh, D.Y., Reinherz, E.L., and Alt, F.W. (1993). Restoration of T cell development in RAG-2-deficient mice by functional TCR transgenes. Science *259*, 822–825.

Takahama, Y., Letterio, J.J., Suzuki, H., Farr, A.G., and Singer, A. (1994). Early progression of thymocytes along the CD4/CD8 developmental pathway is regulated by a subset of thymic epithelial cells expressing transforming growth factor beta. J. Exp. Med. *179*, 1495–1506.

Ueno, T., Hara, K., Willis, M.S., Malin, M.A., Hopken, U.E., Gray, D.H., Matsushima, K., Lipp, M., Springer, T.A., Boyd, R.L., et al. (2002). Role for CCR7 ligands in the emigration of newly generated T lymphocytes from the neonatal thymus. Immunity *16*, 205–218.

Ueno, T., Saito, F., Gray, D.H., Kuse, S., Hieshima, K., Nakano, H., Kakiuchi, T., Lipp, M., Boyd, R.L., and Takahama, Y. (2004). CCR7 signals are essential for cortex-to-medulla migration of developing thymocytes. J. Exp. Med. *200*, 493–505.

Ushiki, T. (1986). A scanning electron-microscopic study of the rat thymus with special reference to cell types and migration of lymphocytes into the general circulation. Cell Tissue Res. *244*, 285–298.

van Ewijk, W., Shores, E.W., and Singer, A. (1994). Crosstalk in the mouse thymus. Immunol. Today *15*, 214–217.

van Vliet, E., Melis, M., and van Ewijk, W. (1984). Immunohistology of thymic nurse cells. Cell. Immunol. *87*, 101–109.

White, S.C., and Casarett, G.W. (1974). Induction of experimental autoallergic sialadenitis. J. Immunol. *112*, 178–185.

Witt, C.M., Raychaudhuri, S., Schaefer, B., Chakraborty, A.K., and Robey, E.A. (2005). Directed migration of positively selected thymocytes visualized in real time. PLoS Biol. *3* (6), e160 DOI: 10.1371/journal.pbio.0030160.

Zuklys, S., Balciunaite, G., Agarwal, A., Fasler-Kan, E., Palmer, E., and Hollander, G.A. (2000). Normal thymic architecture and negative selection are associated with Aire expression, the gene defective in the autoimmune-polyendocrinopathy-candidiasis-ectodermal dystrophy (APECED). J. Immunol. *165*, 1976–1983.

FEBS Letters 580 (2006) 3699–3705

A novel apoptosis cascade mediated by lysosomal lactoferrin and its participation in hepatocyte apoptosis induced by D-galactosamine

Nobuhiko Katunuma[a,*], Quang Trong Le[a], Etsuko Murata[a], Atsushi Matsui[a], Eiji Majima[b], Naozumi Ishimaru[c], Yoshio Hayashi[c], Atsushi Ohashi[a]

[a] *Institute for Health Sciences, Tokushima Bunri University, 180 Nishihamabouji, Yamashiro-cho, Tokushima 770-8514, Japan*
[b] *APRO Life Science Institute, 124-4 Itayashima, Myojin, Seto-cho, Naruto City, Tokushima 771-0360, Japan*
[c] *School of Dentistry, Tokushima University, 3-18-15 Kuramoto-cho, Tokushima 770-8504, Japan*

Received 12 April 2006; revised 25 May 2006; accepted 26 May 2006

Available online 5 June 2006

Edited by Vladimir Skulachev

Abstract **A new apoptosis cascade mediated by lysosomal lactoferrin was found in apoptotic liver induced by D-galactosamine. Caspase-3 and lactoferrin were increased in the apoptotic liver cytoplasm and serum transaminases were elevated. Recombinant lactoferrin stimulated procaspase-3 processing at 10^{-6}–10^{-7} M to an extent similar to that by granzyme B in vitro. Lactoferrin changed procaspase-3 structure susceptible to the processing. Synthetic peptide Y_{679}-K_{695} in lactoferrin molecule inhibited the processing of procaspase-3 by lactoferrin. Lactoferrin in lysosomes was decreased and lactoferrin released into cytoplasm was increased quantitatively in D-galactosamine induced apoptotic liver, and procaspase-3 in cytoplasm was processed to caspase-3.**

Keywords: Apoptosis; Procaspase-3; Lactoferrin; Processing; Lysosome; D-Galactosamine

1. Introduction

Many apoptosis cascades have been reported, and mitochondrial factor mediated apoptosis cascades have been well established. Caspase-3 plays a central role in various apoptosis cascades as an executive enzyme [1–4]. In 1998, we found that an unknown protein extracted from lysosomes by digitonin enhanced procaspase-3 processing in liver cytoplasm [5,6]. After that, we determined that the activating factor was lactoferrin and suggested preliminary the existence of a new apoptosis cascade mediated by lysosomal lactoferrin [7]. This paper reports on the stimulation mechanisms of procaspase-3 processing by lactoferrin at the enzymological aspects in detail and the releasing mechanism of lysosomal lactoferrin into cytoplasm in D-galactosamine-induced apoptotic hepatocyte. The pathological aspects of severe liver injury induced by D-galactosamine have been well characterized by TUNEL staining and also DNA fragmentation [9–11]. We reported in a previous paper that caspase-3 in the cytoplasm of apoptosis liver induced by D-galactosamine was increased and the apoptosis was protected by epigallo-catechin gallate in green tea which inhibited caspase-3 [11].

As the next step, we studied the molecular mechanism underlying increases in the activity of activated caspase-3 in the cytoplasm in vivo and found that a new procaspase-3 activating protein was released into the cytoplasm from lysosomes in D-galactosamine induced apoptotic hepatocytes. We determined that this activating protein was a lactoferrin originally located in lysosomes. Recombinant pure lactoferrin was found to strongly stimulate procaspase-3 processing to form active caspase-3 as same extent to that by granzyme B in vitro, and the activation mechanisms were studied at the molecular level. We reported that releasing mechanism of lysosomal lactoferrin into the cytoplasm in D-galactosamine induced apoptotic rat liver in vivo.

This paper reports on (1) stimulation mechanism of procaspase-3 processing by lactoferrin in vitro; (2) the mechanism by which lysosomal lactoferrin is released into the cytoplasm after D-galactosamine administration in vivo; (3) the existence of a novel apoptosis cascade mediated by lysosomal lactoferrin.

2. Materials and methods

2.1. Chemicals used

Caspase-3, procaspase-3, lipopolysaccharide (LPS), and lactoferrin were all recombinant pure proteins purchased from Sigma Co. (USA). The 17 residue peptide Y_{679}-K_{695} (YEKYLGPQYVAGITNLK) of the lactoferrin molecule was chemically synthesized by Asahi Techno-glass (Chiba, Japan) with 95% purity. Aspartylglutamylvalinylaspartyl-7-amino-4-trifluoromethylcoumarin (DEVD-AFC) was purchased from Peptide Institute Inc., Osaka, Japan.

2.2. Assay of procaspase-3 processing activity

Caspase-3 activity derived from procaspase-3 was determined from the fluorescence of AFC released from DEVD-AFC [5,11], and the enzyme activity was expressed in terms of AFC released in nmol/h/μg protein or nmol/h [5,6,11]. The DEVD-AFC cleavage reaction catalysed by caspase-3 and procaspase-3 processing reaction had the same optimum pH. The rate of fluorescent AFC production from the substrate DEVD-AFC by active caspase-3 was much faster than the rate of processing reaction of procaspase-3 at the optimum pH of 7.5. AFC production could be expressed as the rate of procaspase-3 processing, because procaspase-3 processing is the rate-determining step. Negative staining of SDS–polyacrylamide gel electrophoresis (PAGE)

*Corresponding author. Fax: +81 88 622 2503.
E-mail address: katunuma@tokushima.bunri-u.ac.jp (N. Katunuma).

Abbreviations: LPS, lipopolysaccharide; AFC, 7-amino-4-trifluoromethyl-coumarin; ML, mitochondria-lysosome; AST, aspartate aminotransferase; ALT, alanine aminotransferase; PAGE, polyacrylamide gel electrophoresis; LRF, lactoferrin releasing factor

0014-5793/$32.00
doi:10.1016/j.febslet.2006.05.057

for the activator sample was performed basically according to the method of Fernandez et al. [12]. The processing activities were assayed in the 78-kDa band eluents after removing SDS with renaturing buffer.

2.3. Detection of procaspase-3 activating protein using fluorescent reverse zymography

Our new double layer fluorescent reverse zymographic method was used for the detection of procaspase-3 activating proteins [21]. The activator sample was applied to a 15% polyacrylamide gel copolymerized with DEVD-AFC as the caspase-3 substrate, and the electrophoresis was performed at 13 mA for 120 min. After removing SDS from the gel with the renaturing buffer (2.5% Triton X-100), the gel was incubated with 100 μM procaspase-3 solution at 37 °C for 30 min. The fluorescent AFC band formed by caspase-3 was detected using a UV-transilluminator [13].

2.4. Determination of amino acid sequence of the activating protein of 78-kDa

The intramolecular sequences of the activating protein isolated from the Zn-negative staining SDS–PAGE was determined using an HP G1005A protein sequencing system according to the Majima's method [14]. The protein in the 78-kDa band was digested with lysyl-endopeptidase and the peptide fragments were separated with reverse-phase HPLC on a TSK gel ODS-120 T column (Tosoh) with a linear gradient of acetonitrile in 0.05% trifluoroacetic acid. The amino acid sequences of the main separated peptides were also determined using Majima's method [14].

2.5. Confocal immunohistochemical analysis of lactoferrin located in liver lysosomes

Confocal immunofluorescence analysis was performed on liver sections from C57BL/6 mice using FITC-labeled anti-lactoferrin pAb (Cappel, Turnhout, Belgium) and PE-labeled anti-Lamp-1 mAb (Santa Cruz Biotechnology Inc., Santa Cruz, CA).

2.6. Method of administration of D-galactosamine with LPS in vivo

Rat liver apoptosis was induced by D-galactosamine treatment using Muntane's method [8] by the intraperitoneal injection of D-galactosamine 0.5 g/kg or D-galactosamine 0.5 g/kg plus LPS 50 μg/kg. Twelve hours after the injection, the rats were sacrificed to prepare the livers.

2.7. Preparation of lysosomes and cytoplasmic fraction of rat liver

The rat liver was gently homogenized with a Teflon pestle in 0.25 M cold isotonic sucrose buffer. The suspension was centrifuged at $3500 \times g$ for 10 min at 4 °C to remove the nucleuses and cells. The supernatant was centrifuged at $25000 \times g$ for 20 min at 4 °C to prepare the lysosome-mitochondrial (ML) fraction, and then to prepare the cytoplasm fraction, the supernatant was further centrifuged at $100000 \times g$ for 60 min to remove the microsomes. To prepare pure lysosomes, a two-phase partition centrifugation method in the presence of 1 mM $CaCl_2$ was used [15]. The lysosomal fractions for the assay of procaspase-3 activation were extracted using a 40 μM digitonin solution with isotonic sucrose buffer.

2.8. Sample preparation for activity assay of the lysosomal procaspase-3 activating protein

The ML fractions of rat liver were extracted with 5 mL of digitonin solution. After concentration to 1 mL, 30 μL portion of the extract was applied to SDS gel to make SDS–PAGE. After removing the SDS, the 78-kDa fractions were eluted from the gel for determination of procaspase-3 activating activity or assay of the lactoferrin protein by the antibody. The activating activities were expressed as the AFC released nM/h/mg protein (cytoplasmic protein, lysosomal protein or SDS–PAGE band protein).

2.9. Statistical analysis

Values for expression are shown as means ± S.D. Quantitative differences between values were statistically analyzed by Dunnett's multiple comparison t test P values <0.01 were considered to be significant.

3. Results and discussion

3.1. Detection of procaspase-3 activating protein in the cytoplasm of D-galactosamine treated apoptotic liver cells

When D-galactosamine was administered intraperitoneally to rats, caspase-3 activity in the liver cytoplasm was elevated in a dose-dependent manner 12 h after injection and cotreatment with LPS enhanced the apoptosis dramatically, as shown in Table 1. The liver injury markers, aspartate aminotransferase (AST) and alanine aminotransferase (ALT), were strongly elevated in the serum. Therefore, the increases of caspase-3 may participate in D-galactosamine induced liver injury [11].

In order to elucidate the mechanism of caspase-3 elevation during the apoptosis, the activation factor of procaspase-3 in the treated liver cytoplasm was determined by the following procedure. Same amounts of cytoplasmic fraction and lyso-

Table 1
Elevation of caspase-3 in liver cytoplasm and translocation of lysosomal lactoferrin from lysosomes into cytoplasm in rat liver induced apoptosis by D-galactosamine

Treatments	Enzymes					
	In liver cytoplasm		In liver lysosomes		In serum	
	Caspase-3 (AFC nM/mg/hr)	Activator, 78 kDa (AFC nM/mg/h)	Activator, 78 kDa (AFC nM/mg/h)	Activator, 35 kDa (AFC nM/mg/h)	AST (IU/l)	ALT (IU/l)
Normal	76.50 ± 9.42	25.0 ± 18.6	612.6 ± 210	100.0	23.37 ± 3.69	4.15 ± 1.17
D-GalN (300 mg/kg)		180 ± 90.0	250.0 ± 150	95.0		
D-GalN (500 mg/kg)	1000.0 ± 360	322 ± 126.0	152.4 ± 60	110.0	247.37 ± 194.07	70.17 ± 51.15
D-GalN (700 mg/kg)		609 ± 40	20.0 ± 15	105.0		
LPS(50 μg/kg)	97.56 ± 21.65				23.33 ± 6.25	6.67 ± 1.25
D-GalN(500 mg) + LPS(50 μg/kg)	5159.73 ± 1250.37	1488.6 ± 576.9	≒0		2154.31 ± 598.02	525.94 ± 140.74

0.5 g/kg of the D-galactosamine plus 50 mg/kg of LPS was intraperitoneally injected to rats, and the 12 h after the injection, the rats were sacrificed. The procaspase-3 activating activities (lactoferrin) translocated from the lysosomes into the cytoplasm in the apoptotic hepatocyte were assayed using the method as follows. The quantitative amounts of the digitonin extracts of the lysosomes or the cytoplasm preparations were applied to make SDS–PAGE, and the procaspase-3 activating activities in the 78-kDa fractions and those in the 35-kDa fractions from the lysosomes, and also those from the cytoplasms were assayed at the same time. Furthermore, these activating protein amounts in the cytoplasm corresponded to the released lactoferrin protein amounts using ant lactoferrin antibody [18]. The activating activities were expressed as the AFC released nM/h/mg protein in the extracts of cytoplasmic protein or lysosomal protein. The reciprocal movements of the lactoferrin (procaspase-3 processing activities) in the lysosomes and the cytoplasm were observed in D-galactosamine dose-dependently. Data are shown as the means ± S.D.: $n = 3$–5, $^{*}P < 0.01$.

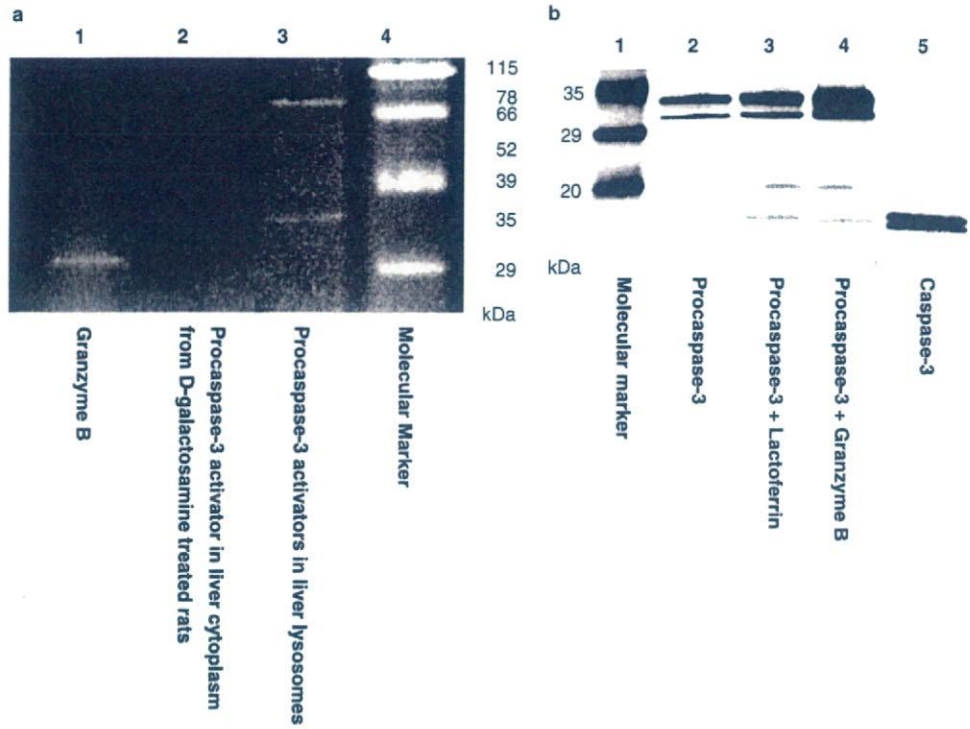

Fig. 1. (a) Detection of procaspase-3 activating proteins in rat liver treated with D-galactosamine using double-layer fluorescent reverse zymography. The procaspase-3 activating proteins were detected using Katunuma's double-layer fluorescent reverse zymography; the method is described in the text [13,21]. DEVD-AFC was used as a caspase-3 substrate. Lane 1: location of granzyme B as the procaspase-3 activating enzyme in the 32-kDa band. Lane 2: Procaspase-3 activating protein in the 78-kDa band was detected in the liver cytoplasm fraction of D-galactosamine treated rats. Lane 3: Procaspase-3 activating proteins in the digitonin extracts of liver lysosome from normal rats in the 78-kDa band which corresponds to the band of lactoferrin and the 35-kDa protein band which is unknown activating protein. (b) Procaspase-3 processing products by lactoferrin. SDS–PAGE gel was stained by Coomassie blue. The products of procaspase-3 processing mediated by lactoferrin were the same as those produced by granzyme B.

somal extract of liver were applied separately to SDS gels and electrophoresis was performed. After removing the SDS from the PAGE with renaturing buffer, the procaspase-3 processing activities in the eluents were detected in the 78-kDa fraction and the 35-kDa fraction using caspase-3 formation from recombinant procaspase-3. The procaspase-3 activating protein in the 78-kDa fraction was increased in the cytoplasm and the activity in the lysosomes was decreased in a reciprocal manner, as shown in Table 1. Sufficient amounts of procaspase-3 were present in the normal cytoplasm, but active caspase-3 was not detected in the normal cytoplasm. These data suggest that the procaspase-3 activating protein is originally located in the lysosomes under normal conditions and that only the 78-kDa activating protein was released into the cytoplasm by D-galactosamine administration.

We then purified the 78-kDa activating protein from the liver lysosomes to allow identification. The partially purified activating protein from the digitonin extracts of liver lysosomes was applied to SDS gels to separate the proteins. Two kinds of activating proteins with molecular weights of 78-kDa and 35-kDa were detected using fluorescent reverse zymography for processing protease detection [13,21], as shown in Fig. 1(a) in lane 3. The 78-kDa band corresponds to recombinant lactoferrin, and the 35-kDa band is an unknown activating protein. The 35-kDa factor was not detected in the cytoplasm of the apoptotic liver, therefore, the 35-kDa factor does not participate in the apoptosis.

3.2. Purification and identification of the 78-kDa lysosomal activating protein as lactoferrin

A procaspase-3 activating protein was extracted with a 40 μM digitonin isotonic sucrose buffer from the purified lysosomes of bovine liver. The specific activity of the procaspase-3 processing enzyme in the digitonin extracts was 2.5 nmol AFC/h/μg protein (formed from DEVD-AFC). The extracted protein was fractionated with 40–60% ammonium sulfate and then heat treated at 70 °C for 1 min. The supernatant was further fractionated with 40–50% ethanol at −20 °C. The fraction was subsequently subjected to column chromatography using Superdex G75, Mono Q and then Hydroxyapatite CHT5-I BIO-RAD. The specific activity of the final active fraction was about 100 nmol AFC/h/μg protein. The purity was increased about 40 times compared with that of the digitonin extracts. The purified sample had about the same activating activity as that of the recombinant pure lactoferrin. The purified fraction showed almost a single protein on the SDS–PAGE.

The intramolecular amino acid sequence of the purified 78-kDa activating protein eluted from the negative zinc staining band in the SDS–PAGE was determined [12]. The sample was hydrolyzed with lysyl-endopeptidase and the peptides produced were separated using reversed-phase HPLC. The amino acid sequences of the two different parts of the separated peptides were determined. The amino acid sequences of these two peptides were completely identical with those of the corresponding parts of recombinant bovine lactoferrin. The amino

acid sequences of these two domains from the purified sample were H_{435}-P_{444} (n-H-S-S-L-D-C-V-L-R-P-c) and N_{653}-E_{661} (n-N-L-L-F-N-D-N-T-E-c). The molecular weight (78-kDa) and the isoelectric point (5.4–5.7) of the purified activating protein were the same as those of the recombinant bovine lactoferrin. The processing product of procaspase-3 by the 78-kDa protein was the same as that by recombinant lactoferrin as demonstrated in Fig. 1(b). The same processing products of procaspase-3 by granzyme B were demonstrated.

3.3. Subcellular localization of lactoferrin in liver lysosomes

A two-phase Ficoll partition centrifugation method in 1 mM $CaCl_2$ was used to determine the subcellular localization of the activating protein in rat liver [15]. The activating activity was detected only in the lysosomal fraction, coinciding with the location of cathepsin L, while the activity was not detected in the swollen mitochondrial fraction, coinciding with glutamic dehydrogenase (data not shown). The confocal immunohistochemical staining of mouse liver, using a monoclonal anti-lactoferrin antibody and a PF-labeled anti-Lamp-1 antibody as lysosomal markers, was used to determine the subcellular localization of the lactoferrin (see Section 2). The lactoferrin was detected only in the lysosomal particles located in the cell membrane area, as Fig. 2 shows.

3.4. Activation mechanism of procaspase-3 by lactoferrin

The activation mode of the procaspase-3 processing reaction mediated by pure lactoferrin was analyzed. Procaspase-3 was originally processed slowly via autocatalytic reaction in Tris–HCl buffer at pH 7.5 and 37 °C in vitro, and 1×10^{-7} M lactoferrin strongly accelerated the autocatalytic processing to several-fold, as shown in Fig. 3(a). The procaspase-3 processing rate mediated by 1×10^{-6} M lactoferrin was about 7000–8000 nM AFC formed per hour, while the autocatalytic rate was about 1000–1600 nM AFC formed per hour. Specific activity of procaspase-3 processing reaction catalyzed by lactoferrin was 432 nM AFC formed/h/mg protein, while that by granzyme B was 515 nM AFC formed/h/mg. Both catalytic activities showed about the same level. The lactoferrin mediated procaspase-3 activating reaction was not inhibited by various cysteine protease inhibitors, including E-64 or serine protease inhibitors, and anti-granzyme B antibody also did not inhibit the activation reaction (data abbreviated). Since both apo-lactoferrin and holo-lactoferrin had the same activation function and 1×10^{-7} M lactoferrin showed the enough activation (Fig. 3(b)), the iron atom itself and the domains of the iron atom binding did not participate in this activation reaction. The processing products of recombinant procaspase-3 mediated by lactoferrin were the same as those mediated by granzyme B by Western blotting using the anti-caspase-3 antibody as shown in Fig. 1(b).

With regard to the activating mechanism of procaspase-3 processing by the lactoferrin, a lactoferrin–procaspase-3 complex may be formed as an intermediate step. The lactoferrin may play a chaperone-like role to alter the tertiary structure of the procaspase-3 and render it more susceptible to being processed. The binding affinity for making the complex was shown in Fig. 3(c), and the K_m is about 1×10^{-11} M. The lactoferrin did not have any effect on the caspase-3 assay reaction. The domain which participates in the binding of procaspase-3 to the lactoferrin molecule was estimated to be Y_{679}-K_{695} (YEKYLGPQYVAGITNLK) in lactoferrin. We reported previously that this domain was an inhibitory site of the

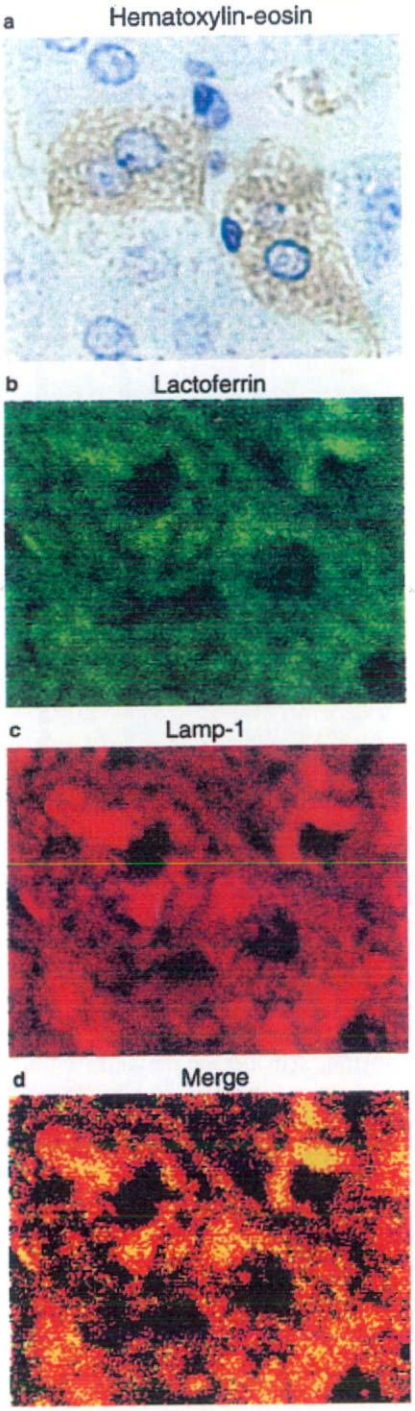

Fig. 2. Subcellular localization of lactoferrin in rat liver using confocal immunohistochemical staining. (a) Hematoxylin-eosin staining of hepatocytes. (b) Lactoferrin localization in lysosomes using an anti-lactoferrin antibody in green. (c) Lysosome staining by PF-labeled-anti-Lamp-1 antibody in red. (d) Merged profile of lactoferrin and lysosomal marker Lamp-1. The lactoferrin was stained in the lysosomes located in the cell membrane area.

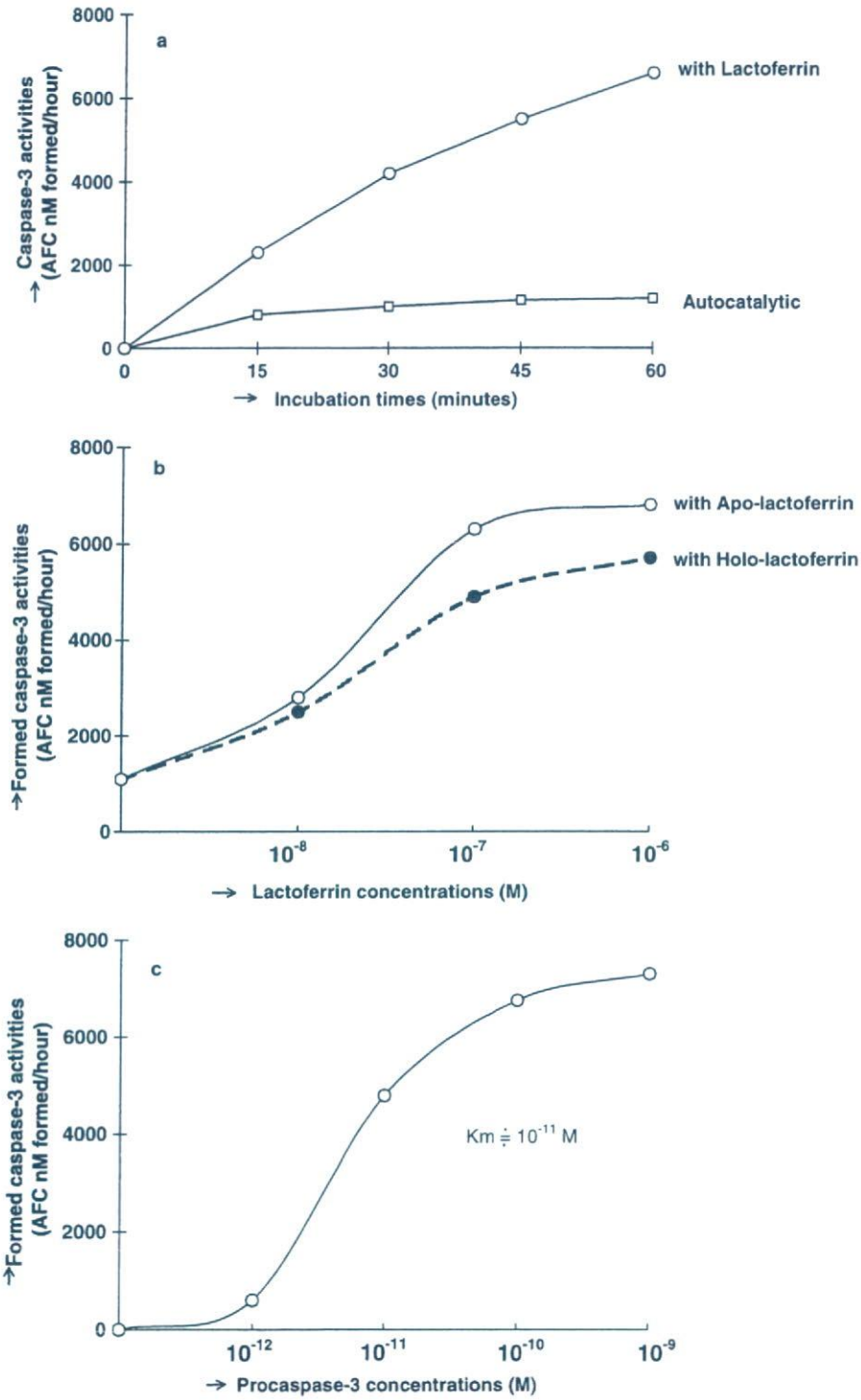

Fig. 3. Activating mechanisms of procaspase-3 processing reaction mediated by lactoferrin. The procaspase-3 processing activity was assayed by the formed caspase-3 activity and the formed caspase-3 activities from procaspase-3 are expressed as AFC formed nM/h in the vertical axis. Panel (a): Reaction time course of procaspase-3 processing with lactoferrin. Panel (b): Dose-dependent activations of the procaspase-3 processing reaction mediated by holo-lactoferrin or apo-lactoferrin. Apo-lactoferrin was prepared from holo-lactoferrin by the treatments at pH 2.0. The iron atoms were released into the supernatant and no iron atoms were detected in the precipitated lactoferrin. Panel (c): Kinetical studies of the affinity of procaspase-3 for lactoferrin and the K_m value.

lactoferrin for cysteine proteases [16]. This domain is highly homologous with a common active site of the cystatin family. The synthetic peptide Y_{679}-K_{695} strongly inhibited not only the activation reaction of the processing mediated by lactoferrin, but also the autocatalytic processing reaction, as shown in Fig. 4. This peptide may disturb the binding of procaspase-3

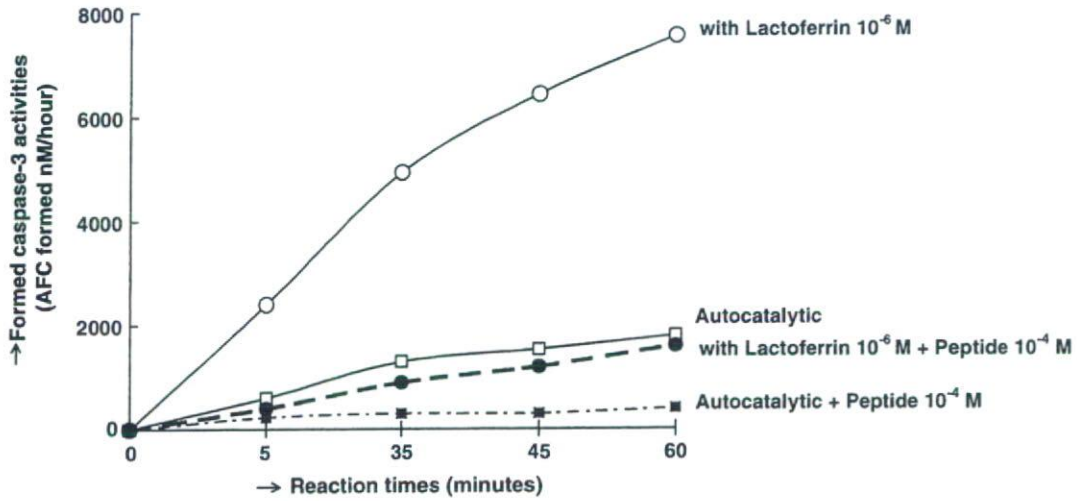

Fig. 4. Inhibition profiles of procaspase-3 processing reaction mediated by lactoferrin by synthetic peptide, Y_{679}-K_{695}, in the domain of lactoferrin molecule. Lactoferrin concentration of 1×10^{-6} M as an activator and synthetic peptide concentration of 1×10^{-4} M as the inhibitor were used. The procaspase-3 processing reaction mediated by 1×10^{-6} M lactoferrin (○–○) and inhibited by 1×10^{-4} M of the peptide (●···●) are shown in this panel. Autocatalytic processing (□–□) and inhibition with 1×10^{-4} M peptide (■···■) are also shown.

to lactoferrin. Therefore, the domain Y_{679}-K_{695} of the lactoferrin may play an important role in the acceleration function by participating in the binding of procaspase-3 to lactoferrin. To explain the practical allosteric structural changes, the X-ray co-crystallographic analysis of these complexes is required. We previously reported a similar type of chaperone-like functioning protein, a chondroitin-sulfate proteoglycan, which is a potent enhancer of the autoprocessing of procathepsin L to form the active mature cathepsin L [17]. We propose that these kinds of specific accelerator proteins, or "enzymoids", may participate in various post-translational processing reactions in general.

3.5. A new apoptosis cascade mediated by lysosomal lactoferrin

To confirm the translocation of the lactoferrin, the lactoferrin released in the cytoplasm was assayed quantitatively with antibodies to lactoferrin using Sanchez's method [18]. The lactoferrin released in the cytoplasm increased to 7 μg/mL of cytoplasm upon treatment with 700 mg/kg D-galactosamine, while no lactoferrin was detected in the normal liver cytoplasm. It is possible to consider that the lactoferrin located in the lysosomes was released into the cytoplasm by D-galactosamine administration dose-dependently in vivo as shown in Table 1, although the releasing mechanisms are not known at the present. The released procaspase-3 activating activity in

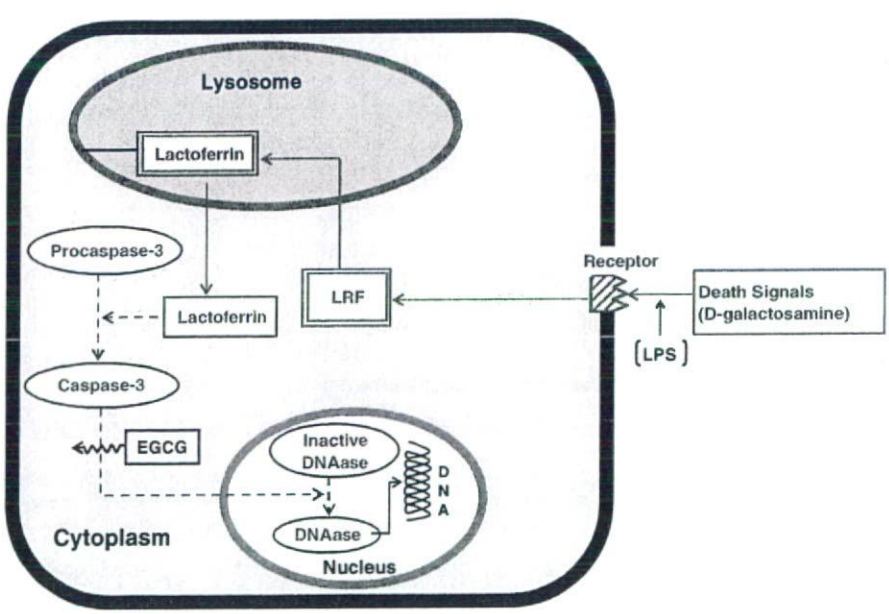

Fig. 5. Schematic illustration of a new apoptosis cascade mediated by lysosomal lactoferrin. Solid red line; the death signal transduction induced by D-galactosamine. Dotted blue line; a new apoptosis cascade mediated by lysosomal lactoferrin. LRF; unknown lactoferrin releasing factor.